Redundant enhancers in the *iab-5* domain cooperatively activate *Abd-B* in the A5 and A6 abdominal segments of Drosophila

Nikolay Postika[1], Paul Schedl[2,3], Pavel Georgiev,[1*] Olga Kyrchanova[1,4*]

[1]Department of the Control of Genetic Processes, Institute of Gene Biology Russian Academy of Sciences, 34/5 Vavilov St., Moscow 119334, Russia;

[2]Laboratory of Gene Expression Regulation in Development, Institute of Gene Biology Russian Academy of Sciences, 34/5 Vavilov St., Moscow 119334, Russia;

[3]Department of Molecular Biology, Princeton University, Princeton, NJ, 08544, USA.

[4] Center for Precision Genome Editing and Genetic Technologies for Biomedicine, Institute of Gene Biology, Russian Academy of Sciences, 34/5 Vavilov St., Moscow 119334, Russia.

*Corresponding author:

E-mail: olgina73@gmail.com (OK)

E-mail: georgiev_p@mail.ru (PG)

Institute of Gene Biology, Russian Academy of Sciences Vavilov Str., 34/5, Moscow, 119334, Russia
+7(499)135-6089

Keywords: */ chromatin boundary / enhancer-promoter interaction / initiator / bithorax / transcription regulation*

Summary Statement

In *Drosophila*, the segment-specific expression of the homeotic gene *Abdominal-B* in the abdominal segments is regulated by autonomous regulatory domains. We demonstrated cooperation between these domains in activation of *Abdominal-B.*

Abstract

The *Abdominal-B* (*Abd-B*) gene belongs to *Bithorax* complex and its expression is controlled by four regulatory domains, *iab-5, iab-6, iab-7* and *iab-8*, each of which is thought to be responsible for directing the expression of *Abd-B* in one of the abdominal segments from A5 to A8. A variety of experiments have supported the idea that BX-C regulatory domains are functionally autonomous and that each domain is both necessary *and* sufficient to orchestrate the development of the segment they specify. Unexpectedly, we discovered that this model does not always hold. Instead, we find that tissue-specific enhancers located in the *iab-5* domain are required for the proper activation of *Abd-B* not only in A5 but also in A6. Our findings indicate that the functioning of the *iab-5* and *iab-6* domains in development of the adult cuticle A5 and A6 in males fit better with an additive model much like that first envisioned by Ed Lewis.

Introduction

In *Drosophila melanogaster* segment identity in the posterior 2/3rds of body is controlled by the three homeotic genes, *Ultrabithorax* (*Ubx*), *abdominal-A* (*abd-A*) and *Abdominal-B* (*Abd-B*), which form the *bithorax* complex (BX-C) (Lewis, 1978). The specification of parasegments (PS)/segment identity depend upon the expression patterns of these three homeotic genes (Duncan, 1987; Karch et al., 1985; Karch et al., 1990; Maeda and Karch, 2015; Peifer et al., 1987). The genes are controlled by an array of nine regulatory domains, each of which is thought to direct the expression of one of the homeotic genes in a spatiotemporal pattern appropriate for the particular PS/segment that the regulatory domain specifies. The *Abd-B* gene, for example, is responsible for the specification/differentiation of PS10/A5, PS11/A6, PS12/A7, PS13/A8. Its expression pattern in each of these parasegments is controlled by four regulatory domains, *iab-5*, *iab-6*, *iab-7* and *iab-8* respectively (Fig. 1A).

Analysis of BX-C regulatory domains, including those controlling *Abd-B* indicate that they are composed of the same set of elements (Kyrchanova et al., 2015; Maeda and Karch, 2015). Each domain has an initiator element that sets the activity state (*on* or *off*) of the domain early in embryogenesis (Maeda and Karch, 2015; Mihaly et al., 2006; Peifer et al., 1987). Initiators responds to the maternal, *gap* and *pair-rule* gene products that subdivide blastoderm stage embryos along the antero-posterior axis into 14 parasegments (Busturia and Bienz, 1993; Casares and Sánchez-Herrero, 1995; Drewell et al., 2014; Ho et al., 2009; McCall et al., 1994; Qian et al., 1991; Shimell et al., 1994; Starr et al., 2011). For example, in PS10/A5, the *iab-5* initiator turns *on* the *iab-5* domain, while the adjacent *iab-6* and other more distal (relative to centromere) domains remain in the *off* state (Iampietro et al., 2010). In PS11/A6, the initiator in *iab-6* turns the domain *on*. While *iab-5* is also active in PS11, *iab-7* and *iab-8* are *off*. The gene products that set the activity state of the BX-C domains disappear during gastrulation and different

mechanisms are deployed to remember the *on* or *off* state. The *on* state is maintained by Trithorax group proteins, while the *off* state is maintained by Polycomb group proteins (Busturia and Bienz, 1993; Kassis et al., 2017; Kuroda et al., 2020; Simon et al., 1992; Shimell et al., 2000; Ciabrelli et al., 2017; Müller and Bienz, 1992). These factors interact with special elements in each domain called Trithorax or Polycomb response elements (TREs or PREs). Finally, each domain has a stage and tissue specific enhancers which are responsible for activating patterns of homeotic gene expression that drive PS/segment differentiation (Maeda and Karch, 2015). Each domain is bracketed by chromatin boundary elements (Barges et al., 2000; Bender and Lucas, 2013; Bowman et al., 2014; Galloni et al., 1993; Gyurkovics et al., 1990; Hagstrom et al., 1996; Iampietro et al., 2010; Karch et al., 1994; Kyrchanova et al., 2020; Mihaly et al., 2006; Zhou et al., 1996). The boundaries in the *Abd-B* region (*Fab-6*, *Fab-7* and *Fab-8*) have two important functions. The first is to block crosstalk between adjacent regulatory domains so that they can function autonomously. The loss of one of these boundaries leads to the ectopic activation/silencing of neighboring regulatory domains. For example, deletion of the *Fab-6* boundary element can result in the ectopic activation of *iab-6* and silencing *iab-5* in PS10/A5 leading respectively to gain-of-function (GOF) and loss-of-function (LOF) transformation of PS/segment (Iampietro et al., 2010; Postika et al., 2021). The second function is boundary bypass. This function enables enhancers in the *Abd-B* regulatory domains to bypass intervening boundaries and activate *Abd-B* (Kyrchanova et al., 2019a; Kyrchanova et al., 2019b; Postika et al., 2018). However, *Fab-7* replacement experiments suggest that bypass activity maybe a special property of the *Abd-B* boundaries as boundaries from elsewhere in the genome do not support bypass (Hogga et al., 2001; Kyrchanova et al., 2019a; Kyrchanova et al., 2019b).

While identity of PS10-PS13/A5-A8 is determined by the pattern of *Abd-B* expression in both sexes, the phenotype of the adult cuticle in segments A5 and A6 in *Drosophila melanogaster* differs in males and females (Jeong et al., 2006; Kopp et al., 2000; Massey and Wittkopp, 2016; Williams et al., 2008). In females, cuticle pigmentation and morphology in A5 and A6 are similar to that in more anterior segments whose identity is determined by *abd-A*. In these segments the tergite has a posterior stripe of dark pigmentation, while the sternite has a quadrilateral shape and has multiple bristles. The pigmented stripe in tergites A2-6 is generated by the *yellow* (*y*) and *tan* genes, which are regulated by the *optomoter blind* (*omb*) gene (Kopp and Duncan, 1997). The *bric-a-brac* (*bab*) complex encodes DNA-binding proteins that repress the expression of the genes responsible for cuticle pigmentation (Couderc et al., 2002; Kopp et al., 2000; Roeske et al., 2018). While female pupae express *bab* in abdominal segments A2–A6, *bab* expression in males is limited to segments A2–A4. The sex specific pigmentation pattern and cuticle morphology in A5 and A6 in males depend upon *Abd-B* and the male product of the *double-sex* gene (dsx^M), which together function to repress expression of *bab* genes in cells giving rise to the A5 and A6 cuticle (Kopp et al., 2000; Massey and Wittkopp, 2016; Wang et al., 2011). *Abd-B* is also thought to

interact with the *y* gene to activate its expression, while it positively regulates *tan* indirectly (Roeske et al., 2018).

The level of *Abd-B* expression in PS10/A5 and PS11/A6 is not the same and correlates with their distinctive morphology. The *Abd-B* expression in A5 is relatively low and this segment has morphological features of the A4 where *Abd-B* is not expressed: the A5 sternite has a quadrilateral shape and has multiple bristles, while the A5 tergite is covered by small trichome hairs. However, due to the expression of *Abd-B* in the A5 segment of males, differences are observed: the sternite becomes wider, the tergite is completely pigmented, and trichomes are less dense (Celniker et al., 1990; Maeda and Karch, 2015) (Fig.1). The higher levels of *Abd-B* in A6 are accompanied by specific morphological features in both the sternite and tergite. The A6 sternite lacks bristles and has a unique 'banana' shape, while the trichomes on the fully pigmented tergite are restricted to the anterior and dorsal margins instead of covering nearly the entire tergite.

Here, we have investigated the mechanisms responsible for regulating *Abd-B* expression during the differentiation of the male cuticle in segments A5 and A6. We have found that *iab-6* is not on its own able to direct expression of *Abd-B* in the manner that is required for differentiation of the A6 cuticle in male flies. Instead, the *iab-5* and *iab-6* domains share a common set of partially redundant cuticle enhancers located in *iab-5* that are critical for male specific differentiation of the cuticle of A5 and A6. In this respect, the functioning of *iab-5* and *iab-6* domains fit well with the additive model for BX-C regulation suggested by Lewis (1978).

Results

Inactivation of the *iab-5* domain affects expression of *Abd-B* in the A6 segment

Experiments in which *Fab-7* was replaced by heterologous boundaries have shown that the three boundaries in the *Abd-B* region of the complex, *Fab-6*, *Fab-7* and *Fab-8* have both blocking and bypass activity (Kyrchanova et al., 2019a; Kyrchanova et al., 2019b; Postika et al., 2018). In contrast, heterologous boundaries such as *scs*, *Mcp* or artificial DNA fragments consisting of multimerized binding sites for C_2H_2 zinc finger proteins like Pita or dCTCF have only blocking activity (Kyrchanova et al 2016; 2017; Hogga et al. 2001). For example, when a multimer consisting of five binding sites for Pita (*Pita*$^{\times 5}$) is used to replace *Fab-7*, the identity of PS12/A7, which is specified by *iab-7*, is the same as in *wild type* (*wt*); however, *Pita*$^{\times 5}$ blocks *iab-6* from activating *Abd-B* in PS11/A6. Instead, *iab-5* regulates *Abd-B* activity in both PS10/A5 (where it normally functions) and PS11/A6 and adult *Pita*$^{\times 5}$ males have a

duplicated A5 segment. While these experiments showed that boundaries at the position of *Fab-7* (between *iab-6* and *iab-7*) must have both blocking and bypass activity for the proper regulation of *Abd-B*, a similar requirement has not been established for boundaries at the location of *Fab-6* or *Fab-8*. To test whether the regulation of *Abd-B* by *iab-5* requires that the boundary located between *iab-5* and *iab-6* must have bypass activity, we took advantage of the $F6^{1attP}$ replacement platform, in which a 1389 bp sequence spanning the *Fab-6* boundary was substituted by an *attP* site (Postika et al., 2021). Reintegration of the 529 bp core *Fab-6* boundary, including two dCTCF sites, completely restored *wt* male phenotype, suggesting that the 1389 bp deletion does not include important regulatory elements other than the *Fab-6* boundary.

We inserted the $Pita^{\times 5}$ insulator into the $F6^{1attP}$ platform. Based on how it functions as a *Fab-7* replacement, we expected that it would block crosstalk between *iab-5* and *iab-6*, but would also prevent *iab-5* from regulating *Abd-B*. To assess the activity state of *iab-5* and *iab-6* cuticle enhancers we included a *mini-yellow* (*mini-y*) reporter which we placed either upstream of $Pita^{\times 5}$ or downstream so that it would be located in the *iab-5* (*mini-y* $Pita^{\times 5}$) or *iab-6* ($Pita^{\times 5}$ *mini-y*) domains, respectively (Fig. S1). The reporter consists of a *yellow* (*y*) cDNA fused to the 340 bp *y* promoter. As it lacks the enhancers of the endogenous *y* gene, its expression depends upon nearby enhancers. Expression of *mini-y* was examined in a y^1 background. In flies carrying the null y^1 allele, the *tan* gene is appropriately expressed in A5 and A6 reflecting the *Abd-B* activity, and the resulting pigmentation in the tergite is light brownish, not black (Camino et al., 2015; Rebeiz and Williams, 2017).

Males homozygous for the starting $F6^{1attP}$ deletion differ from *wt* in that segment A5 has an incomplete GOF and LOF transformation (Fig. 1). The A5 sternite has a shape like that normally observed in A6, but with several bristles, the A5 tergite has patches of cuticle that lack trichomes, which is indicative of a GOF transformation towards A6 identity. On the other hand, large portions of the A5 cuticle also lack *tan* pigmentation, indicating that the cells have an A4 identity. There are also unexpected (based on *Fab-7* and *Fab-8* boundary deletions: Mihaly et al., 1997; Barges et al., 2000) LOF phenotypes in A6 including bristles on the sternite and regions of the tergite that are depigmented or have ectopic trichomes.

As expected, the $Pita^{\times 5}$ replacement (with or without *mini-y*) blocks crosstalk between *iab-5* and *iab-6* and the GOF transformations of A5 are eliminated (Fig. 1). In addition, consistent with idea that a boundary located between *iab-5* and *iab-6* must have bypass activity, A5 resembles A4: the sternite has a quadrilateral shape, and is covered in bristles, while the tergite is covered in trichomes, and instead of being covered in pigmentation, there is only a posterior stripe. This result shows that *iab-5* is unable to activate *Abd-B* in A5 when $Pita^{\times 5}$ is present.

However, there is also an unexpected result: the differentiation of A6 is altered compared to *wt*. The defects are most clearly evident when *mini-y* is excised and y^+ allele is introduced. Fig. 1 shows that pigmentation of the A6 tergite resembles A4: there is only a stripe of pigment along the posterior margin of the tergite. In addition, the A6 tergite is covered in trichomes just like A4. While the A6 sternite has a nearly normal shape, there are multiple bristles. These LOF transformations indicate that the $Pita^{\times 5}$ insulator disrupts *Abd-B* dependent cuticle differentiation not only in A5, but also in A6. Since the insulator is located between *iab-5* and the *Abd-B* gene this would imply that it is blocking enhancers in *iab-5* that are required for the proper activation of *Abd-B* in the cells that form the A5 and also the A6 cuticle in males.

Further support for this conclusion comes from analysis of *mini-y* expression in the y^1 background. In $Pita^{\times 5}$*mini-y* males the reporter located in the *iab-6* domain it is not turned on in either in A5 or in A6. Instead, only the *tan* gene is expressed, and importantly it is expressed in an A4 like pattern. This result would indicate that enhancers in *iab-5* are required to drive expression of *mini-y* inserted in *iab-6* in the A6 tergite. Finally, when the *mini-y* reporter is in *iab-5* we observe a mosaic pattern of pigmentation in the posterior stripes of the A4, A5 and A6 segments regulated by *omb*, but not *Abd-B*.

The *iab-5* domain contains a set of redundant cuticle enhancers that can drive *yellow* expression outside BX-C

To map enhancers in the *iab-5* regulatory domain responsible for *Abd-B* expression in the cells that give rise to the male cuticle in A5 and A6, we linked 1-3 kb overlapping DNA sequences from the *iab-5* domain ($i5^1$ – $i5^7$ and $i5^{ini}$ (Busturia and Bienz, 1993)) to a *y* reporter in a transgene that also carries a *mini-white* (*w*) (Fig. 2, Fig. S2). To reduce potential position effects, we placed $Pita^{\times 5}$ upstream of the *iab-5* DNA fragments. Using *phiC31*-mediated recombination (Gao et al., 2008), we integrated a collection of eight *i5* transgenes into a well characterized 86Fb platform (Bischof et al., 2007). Of these *i5* fragments, only three, $i5^1$ (1013 bp), $i5^2$ (2145 bp) and $i5^7$ (2524 bp), activated *y* expression in the cuticle (Fig. 2, Fig. S2). For all three, pigmentation was observed in the A5 and A6 tergites. Interestingly, we found that the $i5^7$ fragment was only able to activate *y* in the forward (genomic) orientation. We tested two $i5^7$ subfragments from the proximal ($i5^{S5}$) and distal ($i5^{S6}$) ends relative to the centromere. Of these, only $i5^{S6}$, activated *y*. Thus, in the larger $i5^7$ fragment, the enhancer in $i5^{S6}$ must be located next to the promoter to function. Since the $i5^1$ and $i5^2$ overlapped, it seemed possible that they share the same enhancer. To test this, we generated three smaller fragments ($i5^{S1}$, $i5^{S2}$, and $i5^{S3}$) spanning most of $i5^1$ and $i5^2$. Of these only $i5^{S2}$ which includes the overlap between $i5^1$ and $i5^2$ activates *mini-y*.

Functioning of the *iab-5* enhancers in the *iab-6* domain

We next determined whether *iab-5* sequences are able to regulate *Abd-B* in A6 when placed in *iab-6*. We used the $F6^{1attP}$ landing platform to insert the same collection of *iab-5* sequences into the *iab-6* regulatory domain (Fig. S3). The transgenes included $Pita^{\times 5}$ to block crosstalk between *iab-5* and testing fragments and excisable *mCherry* and *mini-y* reporters arranged so that in the replacement they are located in *iab-6* (Fig. S1).

Three of the *iab-5* sequences, $i5^{1}$, $i5^{3}$, and $i5^{7}$ are able to stimulate *mini-y* expression to different extents in the A6 segment (Fig. S3). While both $i5^{1}$ and $i5^{7}$ also stimulated *y* when inserted in 86Fb platform, $i5^{3}$ did not (Fig. 2). Conversely, $i5^{2}$ failed to function when placed in *iab-6*, while it is active in the 86Fb platform. It seems likely that "position effects" are responsible for the differences in the activity of the *iab-5* sequences when linked to the *y* reporter in 86Fb or inserted in *iab-6*. As would be expected from their placement in *iab-6*, $i5^{1}$, $i5^{3}$ and $i5^{7}$ do not activate the reporter in more anterior segments. Surprisingly, insertion of the $i5^{7}$ fragment in the reverse orientation ($i5^{7R}$) stimulates *mini-y* expression in posterior stripes not only in the A6 tergite, but also in the A5 and A4 tergites (Fig. S3). Since the distal part of $i5^{7}$, $i5^{S6}$, induces a much stronger activation of the *mini-y*, it would appear that sequences elsewhere in $i5^{7}$ contain a silencer.

As the reporters compete with *Abd-B* for enhancer activity we assessed the cuticle phenotypes after removing the reporters and introducing a y^{+} allele (Fig. 3). When $i5^{1}$, $i5^{3}$ or $i5^{7}$ are included in the $Pita^{\times 5}$ replacements the phenotype of A6 is close to *wt*. Even though $i5^{S2}$ and $i5^{2}$ activate *mini-y* at 86Fb, neither could rescue the LOF phenotypes induced by $Pita^{\times 5}$. On the other hand, $i5^{S1}$ and $i5^{3}$, which does not stimulate *mini-y* at 86Fb, completely rescues the $Pita^{\times 5}$ induced LOF phenotypes in A6 (Fig. 2, 3). The remaining fragments that are active when introduced into *iab-6* are $i5^{ini}$ and $i5^{7}$. The former is not active at 86Fb, while the latter is. Both partially rescue the $Pita^{\times 5}$ induced defects in pigmentation and trichome distribution in A6, while the weak LOF phenotype (bristles) in the sternite are rescued by $i5^{7}$ but not $i5^{ini}$. As was the case in 86Fb, the $i5^{7}$ enhancer activity is orientation dependent and it is not observed in $i5^{7R}$. Thus, there are several enhancers in *iab-5* that could help drive *Abd-B* expression in the cuticle and generate morphological features that are characteristic of A6.

Deletion of the *iab-5* initiator disrupts morphology of the A5 and A6 segments

The results in the previous section indicate that enhancers in *iab-5* are important for the proper differentiation of the adult cuticle in A6. If this suggestion is correct, one would predict that the deletion of the *iab-5* initiation element will disrupt the development of the adult cuticle not only in A5 but also in

A6. To test this prediction, we used CRISPR/Cas9 to delete a 1975 bp genomic DNA segment that spans the *iab-5* initiator (Busturia and Bienz, 1993) and replace it with an *attP* site and an excisable *dsRed* reporter under control of the *3×P3 hsp70* promoter (Fig. S1). As expected for an initiator deletion, the A5 segment in $i5^{attP}$ males resembles A4 (Fig. 4, Fig. S4 and S5). Critically, this is not the only phenotypic alteration in $i5^{1attP}$ males. Instead of the characteristic banana shape, the A6 sternite has an intermediate quadrilateral shape and also has bristles, while the A6 tergite has an irregular and variable pigmentation. In addition, trichome hairs are found in large patches often coinciding with areas of depigmentation. These results show that deletion of the *iab-5* initiator affects *Abd-B* expression in both the A5 and A6 segments. To confirm that *iab-5* is not properly activated in $i5^{1attP}$ we integrated a *mini-y* reporter using the *attP* site. As expected, the *mini-y* reporter introduced into *iab-5* is *off* in A5. In A6, black pigmentation is restricted to several patches on the tergite, while *tan*-only dependent pigmentation occupies a somewhat larger area (Fig. 4, Fig. S5).

To confirm that the observed effects on *mini-y* and A6 morphology are induced by deletion of the *iab-5* initiator, we introduced a 1025 bp $i5^{ini}$ fragment together with *mini-y* into $i5^{1attP}$. The resulting flies have *wt* morphology except for 1-2 bristles on the A6 sternite, and the *mini-y* reporter is expressed throughout the tergite in A5 and also A6 (Fig. 4). The presence of bristles on the A6 sternite is due to competition between the *mini-y* and *Abd-B* promoters.

Creation of a platform for testing the functional role of regulatory elements in *iab-5*

To further evaluate the functional role of the *i5* enhancers in both A5 and A6, we have created a platform by deletion most of *iab-5* sequence to test the functional role of individual *i5* regulatory elements and their various combinations. For this purpose, we used Cre-mediated recombination between *lox* sites located in the $i5^{attP}$ and an *Mcp* boundary deletion, M^{3attP}, in which a 3,333 bp sequence spanning the region around the *Mcp* boundary was substituted by *attP* and *lox* sites (Fig. 4, Fig. S6 and S7). After Cre recombination, the final deletion, $M\text{-}i5^{attP}$, is 10935 bp. It extends from the centromere proximal side of the *Mcp* boundary through the *iab-5* initiator, leaving the 2126 bp $i5^{7}$ sequence (Fig. 4) and single *attP* and *lox* sites. $M\text{-}i5^{attP}$ males have a pigmented A4 segment and display other signs of GOF transformation of not only A4 and A5, but also A3: the sternites have two lobes somewhat like the A6 sternite, while there is a depletion of the trichomes on the tergites (Fig. 4, Fig. S4).

Aiming to prevent the *iab-4* domain from activating *Abd-B*, we reintroduced a M^{413} insulator, characterized previously (Kyrchanova et al., 2007), with the *mini-y* reporter using the *phiC31* integration system (Fig. S1). The resulting M^{413}*mini-y* replacement contains only the $i5^{7}$ sequence. As would be expected since there is no initiator in *iab-5*, the domain is inactive in A5 and *mini-y* is not expressed in this

segment. However, in spite of the fact that the *iab-5* domain is inactive, the phenotype of A6 resembles *wt* and the *mini-y* reporter, which is located in the inactive *iab-5* domain, is expressed throughout the A6 tergite (Fig. 4). When the reporters are excised, the minimal Mcp^{413} boundary is not able to prevent *iab-4* from activating the enhancer in $i5^{7}$, or *Abd-B* directly. In addition to having a *wt* A6 segment, the tergites in A4 and A5 are nearly covered in pigmentation indicating that the *Abd-B* gene active in both of these segments (Fig. S8).

A plausible interpretation of these findings is that the *iab-4* domain somehow activates the remaining *iab-5* enhancers ($i5^{7}$) in this deletion. To test the possible role of the *iab-4* regulatory region in the GOF transformation of A4 in Mcp^{413}, we deleted a 4,401 bp sequence ($iab\text{-}4^{\Delta}$) including the *iab-4* initiator as described previously (Postika et al., 2018). The deletion of these *iab-4* sequences not only reverts the GOF transformations in M^{413}, but also results in a dramatic LOF transformation of *both* A5 and A6 (Fig. 4). While A5 resembles A4 in $M^{413}iab\text{-}4^{\Delta}$ males, the pigmentation patterns in the A6 tergite range from a few dark spots to almost ubiquitous pigmentation (Fig. S9). The A6 sternite is also misshapen and covered in bristles. Since A6 appears *wt* when the *iab-4* domain is intact, it would appear that in the M^{413} platform sequences in *iab-4* are able, either on their own or in collaboration with elements in *iab-6* to activate enhancers in $i5^{7}$, and help direct the proper expression of *Abd-B* in A6.

Reconstructing a minimal *iab-5* domain

We next used the $M\text{-}i5^{attP}$ platform to reconstruct a minimal *iab-5* regulatory domain. Since Mcp^{413} in combination with the two reporters is more effective in insulating against elements in *iab-4*, we will first consider the functioning of different *iab-5* sequences in the presence of the reporters. In the first set of experiments, we tested $i5^{S2}$ and $i5^{3}$. Since the $M\text{-}i5^{attP}$ deletion retains the $i5^{7}$, it is included in all of the replacements we tested. Thus, the three combinations are $i5^{S2}{+}i5^{7}$; $i5^{3}{+}i5^{7}$ and $i5^{S2}{+}i5^{3}{+}i5^{7}$ (Fig. 5). In both $i5^{7}$ and $i5^{S2}{+}i5^{7}$ the *mini-y* reporter is expressed in a mosaic pattern along the posterior margin of A4 and A5. In contrast, we observed only rare spots of dark pigmentation in the A5 segment in combinations containing $i5^{3}$. Thus, the $i5^{3}$ region has a negative effect on *mini-y* expression in *cis*. In all three combinations ($i5^{S2}{+}i5^{3}{+}i5^{7}$), the anterior 2/3rds of A5 tergite is largely devoid of pigmentation, indicating that the *tan* gene is also not expressed in much of the tergite. At the same time, the A6 segment has a nearly *wt* phenotype.

We next tested the same combinations of *i5* enhancers with the initiator, $i5^{ini}$. The $i5^{ini}{+}i5^{7}$ combination expands the expression domain of *mini-y* in A5, while having minimal effect on expression in A4. However, there are regions in the anterior of the A5 tergite where *mini-y* is not expressed (Fig. 5).

While adding $i5^{S2}$ has little effect on the pattern of *mini-y* expression ($i5^{S2}$+$i5^{ini}$+$i5^{7}$), there is a noticeable expansion in the expression area in A5 when $i5^{3}$ is combined with the initiator ($i5^{3}$+$i5^{ini}$+$i5^{7}$) (Fig. 5). This is the opposite of what was observed for $i5^{S2}$+$i5^{S7}$ and $i5^{3}$+$i5^{S7}$combinations without the initiator sequence. However, even in this case, *mini-y* expression is not observed throughout the A5 tergite. On the other hand, when the initiator is combined with all three sequences ($i5^{S2}$+$i5^{3}$ + $i5^{ini}$+$i5^{7}$), *mini-y* is expressed throughout the entire A5 tergite as is *tan*, while the ectopic activation in A4 is absent. (Fig. 5). Thus, this combination appears to be sufficient for full domain function.

We also examined the activity of the *iab-5* enhancers after reporter excision (Fig. S8). The GOF transformations (misshapen sternites and loss of trichome hairs) in the morphology of segments A3-6 in the starting *M-*$i5^{attP}$ platform are largely rescued by the introduction of the *Mcp* insulator, M^{413}. However, as mentioned above, the pigmentation patterns in A4 and A5 are still abnormal. The former has patches of ectopic pigmentation, while the latter is not fully pigmented. The pigmentation patches in anterior of A4 and A5 mostly disappear in the $i5^{S2}$+$i5^{7}$ combination. When $i5^{S2}$+$i5^{7}$ are combined with $i5^{3}$ there is a further suppression in A5 pigmentation, and a loss of pigmentation in A4. Thus, the $i5^{3}$ and $i5^{7}$ sequences, in cooperation $i5^{S2}$, can block the activation of *Abd-B* expression mediated by sequences in the *iab-4* domain. However, as was observed when *mini-y* is present, the *iab-5* enhancers in $i5^{S2}$, $i5^{3}$ and $i5^{7}$ are unable to direct the proper development of A5 unless the *iab-5* initiator is also present. Addition of $i5^{ini}$ to $i5^{7}$, or $i5^{S2}$+$i5^{7}$, or $i5^{3}$+$i5^{7}$ substantially expands the area of pigmentation not only in the A5 tergite, but also in A4 (Fig. S8). As was observed for the *mini-y* reporter, combining $i5^{ini}$ with $i5^{S2}$+$i5^{S3}$+$i5^{S7}$ gives what appears to be a fully *wt* pattern of pigmentation in both A4 and A5. Thus, the $i5^{S2}$+$i5^{S3}$+$i5^{S7}$ combination blocks incorrect activity of the *iab-4* and *iab-5* initiators in the A4 segment and is sufficient in cooperation with $i5^{ini}$ for the proper stimulation of *Abd-B* in the A5 segment.

Discussion

The temporal and spatial patterns of expression of the three BX-C homeotic genes are generated by nine regulatory domains that are arranged in the same order in the chromosome as the PS/segments that they are thought to specify (Duncan, 1987; Karch et al., 1985; Peifer et al., 1987). Two different models have been proposed to explain the functional properties of these regulatory domains. In the first, the additive model, which was envisioned nearly fifty years ago by Lewis (1978), the regulatory domains for each PS/segment are sequentially activated from anterior to posterior along main body axis. Once activated, the domain is also active in all of the more posterior PS/segments and thus could contribute to the differentiation of more posterior segments. This would mean that while each domain is necessary for specifying the identity and directing the differentiation of a specific PS/segment, it may not be sufficient.

In the case of *Abd-B*, for example, it first turns on in PS10/A5. In this PS/segment, the *iab-5* domain is responsible for controlling *Abd-B* expression and it would be both necessary and sufficient for differentiation of this PS/segment. This would not be true for *iab-6*, which is activated in the next posterior PS11/A7. While *iab-6* would be necessary for the differentiation of PS11/A6, it would not be sufficient. Instead, differentiation would require the combined action of enhancers in *iab-6* and *iab-5* (Fig. 6). For the next posterior PS12/A7, the *iab-7* domain would be essential for differentiation; however, the requisite pattern of *Abd-B* expression would only be achieved by the contributions of *iab-5* and *iab-6*. Several lines of evidence are consistent with this model. Antibody staining experiments in the embryo showed that the levels of Abd-B and the number of cells expressing this protein increase in a stepwise fashion between PS10 and PS12 (Celniker et al., 1990; Delorenzi and Bienz, 1990; Sánchez-Herrero, 1991). It also fits with the finding that mutations which inactivate an *Abd-B* regulatory domain result in an LOF transformation in which the PS/segment assumes the identity of the immediately anterior PS/segment. For example, an $iab\text{-}6^{4}$ deletion (Iampietro et al., 2010), transforms PS11 in copy of the more anterior PS10. Similarly, an *iab-7* deletion, $iab\text{-}7^{Sz}$, transforms PS12 in copy of the PS11 (Mihaly et al., 1998). In the additive model, this transformation arises because *iab-5* and *iab-6* already have a role in activating *Abd-B* in PS12/A7 together with *iab-7* in *wt*. In the $iab\text{-}7^{Sz}$ mutant, they still have this function in PS12/A7, but are only able to drive a pattern of *Abd-B* expression appropriate for PS11/A6 identity/differentiation. This model leaves open the question of whether the enhancers in different domains are strictly additive or have complementary activities. In the former case, the enhancers in, for example, *iab-5*, would work in concert with enhancers in *iab-6* to generate a higher level of *Abd-B* expression in each cell in PS11/A6. Consistent with the notion that there are redundant tissue specific enhancers spread throughout the complex, Crosby et al showed that a deletion which removes sequences extending from *iab-4* to *iab-7* induces the segments A4 through A7 to assume an A6-like identity (Crosby et al., 1993). In the latter case, the enhancers in *iab-5* would drive expression in the same set of cells in both PS10/A5 and PS11/A6. The enhancers in *iab-6* would then be responsible for activating *Abd-B* in a set of cells that do not express *Abd-B* in PS10/A5. Consistent with this idea, a comparison of the pattern of Abd-B expression in the embryonic CNS in PS10 and PS11 suggests that there are greater number of Abd-B positive cells in PS11.

In the second model each regulatory domain is both necessary and sufficient to drive the expression of one of the homeotic genes in a pattern appropriate for the differentiation of give PS/segment (Peifer et al., 1987; Simon et al., 1990). A number of observations support the notion that BX-C regulatory domains are sufficient on their own to specify segment identity/differentiation. The first comes from deletions that span *iab-5* and *iab-6* (Mihaly et al., 2006). While these deletions transform both PS10/A5 and PS11/A6 towards a PS9/A4 identity, they have no apparent effect on the differentiation of

PS12/A7. The second comes from boundary replacement experiments. Deletions of *Fab-7* transform PS11/A6 into a copy of PS12/A7, but have no discernable effect on the development of PS12/A7. Hogga et al (2001) showed that this GOF transformation can be rescued by the *scs* boundary (Hogga et al., 2001); however, unlike *Fab-7*, *scs* prevents *iab-6* from regulating *Abd-B*, and PS11/A6 is transformed into a copy of PS10/A5. Importantly, though *iab-6* is prevented from regulating *Abd-B*, this has no effect on the development of PS12/A7. This result indicates that *iab-7* is sufficient on its own to direct a pattern of *Abd-B* expression appropriate for the differentiation of PS12/A7. Subsequent experiments in which *Fab-7* was replaced by a variety of different boundaries that lack bypass activity, but block crosstalk have supported this conclusion (Hogga et al., 2001; Kyrchanova et al., 2016; Kyrchanova et al., 2017; Kyrchanova et al., 2019a).

One of the boundaries tested in these *Fab-7* replacement experiments was *Pita*$^{\times 5}$ (Kyrchanova et al., 2017; Kyrchanova et al., 2019a). Like other heterologous boundaries, it blocks crosstalk between *iab-6* and *iab-7* and rescues the GOF transformation of the *Fab-7* boundary deletion. However, it lacks bypass activity and PS11/A6 assumes a PS10/A5 identity. PS12/A7, on the other hand, is specified correctly. As shown here, it functions in a similar fashion when used to replace the *Fab-6* boundary. It blocks crosstalk between *iab-5* and *iab-6* and rescues the transformations of PS10/A5 induced by the deletion. At the same time, PS10/A5 assumes a PS9/A4 identity. This is the result expected for a boundary element at the position of *Fab-6* that fails to support bypass of the *iab-5* regulatory domain. However, unlike the *Pita*$^{\times 5}$ replacement of *Fab-7* which has no effect on the specification of PS12/A7, the *Pita*$^{\times 5}$ replacement of *Fab-6* also disrupts the development of PS11/A6. Just like PS10/A5, the pigmentation of the PS11/A6 tergite and the pattern of trichome hairs resemble that seen in PS9/A4 in *wt* males. Since insulators must be interposed between enhancers/silencers and promoters in order to block regulatory interactions, the defects in the differentiation of the cuticle in PS11/A6 in adult males cannot be due to insulator dependent interference with the cuticle enhancers in *iab-6*. Instead, *Pita*$^{\times 5}$ has to block enhancers in *iab-5* from correct regulation of *Abd-B* not only in PS10/A5, but also in PS11/A6. This conclusion is supported by two other results. First, the defects in A6 induced by replacing *Fab-6* with *Pita*$^{\times 5}$ can be partially or completely rescued by introducing several different *iab-5* sequences into *iab-6*. This finding indicates that there are cuticle enhancers in *iab-5* that can support the proper differentiation of the A6 tegerite if they are not blocked by the *Pita*$^{\times 5}$ insulator. Second, deletion of the *iab-5* initiator expectedly inactivates the *iab-5* domain, and A5 is transformed into a copy of A4, however, the partial LOF transformation of A6 is also observed. These LOF transformations indicate that the formation of the characteristic sex-specific cuticular features in the A6 segment requires regulatory elements located in *iab-5*. Taken together, these findings indicate that *iab-6* is not on its own able to direct expression of *Abd-B* in the manner that is required for differentiation of the A6 cuticle in male flies. Instead, the adjacent *iab-5* domain is needed to

supplement the intrinsic enhancer activities of the *iab-6* domain. In this respect, the functioning of *iab-5* and *iab-6* domains fit well with the model for BX-C regulation suggested by Lewis (1978). On the other hand, this does not seem to be true for *iab-7* which appears to be both necessary and sufficient for the development of PS12/A7 (Fig. 6).

While our results demonstrate that the proper differentiation of A6 requires several distinct enhancers in *iab-5* to drive *Abd-B* expression in the appropriate manner, the *iab-5* domain cannot on its own substitute for *iab-6*. Experiments by Iampietro et al (2010) showed that deletion of the *iab-6* initiator results in a LOF transformation of A6 into A5. Thus, it is possible that the differentiation of the A6 cuticle in adult males requires that enhancers in *iab-5* and *iab-6* work in concert (Fig. 6). In the case of *iab-5*, we have found that at least four distinct DNA sequences ($i5^{S2}$, $i5^{3}$, $i5^{7}$ and the *iab-5* initiator $i5^{ini}$) are required for proper differentiation of A5. Several lines of evidence (orientation or position dependent activation of the *yellow* reporter) suggest that the $i5^{S2}$, $i5^{3}$ and $i5^{7}$ sequences contain not only tissue-specific enhancers but also silencers that are not coincide with regions bound by Polycomb proteins (Fig. 2). With respect to the cells in the cuticle in which these enhancers/silencers are active, it would appear that they have overlapping rather than completely distinct activities. The *i5* sequences also seem to help the Mcp^{413} boundary block interactions between the *iab-4* and *iab-5* initiators/regulatory elements. At this point it is not yet clear whether there are also multiple, physically distinct cuticle enhancers in *iab-6*. Even if this is not true, it would appear that *Abd-B* expression in the cells in PS10 and PS11 that give rise to adult male cuticle in A5 and A6 depends on interactions with several physically distinct enhancer elements. Whether these interactions occur simultaneously, or only individually remains to be determined. Likewise, it is not clear whether the effects are strictly additive, or whether the enhancers in *iab-5* are active in sets of cells that are distinct from the cells in which the *iab-6* enhancers are active.

Methods

Generation of $i5^{1attP}$, M^{3attP} and $M\text{-}i5^{attP}$ platforms

The deletions were obtained by CRISPR/Cas9 method (SI Appendix, Fig. S1). As a reporter, we used *pHD-DsRed* vector (Addgene plasmid # 51434). The plasmid was constructed in the following order: *proximal arm-attP-lox-3×P3:DsRed-SV40polyA-lox-distal arm*. Arms were amplified by PCR from DNA isolated from *Oregon* line. For generation of the $i5^{1attP}$ deletion, homology arms were obtained by DNA amplification between primers: TGTCGAGGTCCCGAAATG and ACGTCACTTGGCTGAAATGC; CAGACAGGTCCATCGGGG and TTGTTGAGGGTTGGTTGTG. For ^{M3attP}: ATAACTAGTCCTAAATTACGACCACGAC and

ATACTCGAGCCCATAAACAGCACGGC; ATAGCGGCCGCATTTTAATCGAGCCATC and CGAGAATTCCTAGAATGAGTAG. The guide RNAs were selected using the program "CRISPR optimal target finder" (O'Connor-Giles Lab). For $i5^{1attP}$ deletion: TTTCGGGACCTCGACACGTT_TGG and TTGGCCCCGATGGACCTGTC_TGG. For M^{3attP}: CACTGACAGAGTCAGGCTCG_TGG and CATACTTGCCCCGTACTTGC_CGG. The breakpoints of the designed deletion: $i5^{1attP}$ - 3R:16877730.. 16879686 (1957 bp) and M^{3attP} - 3R:16872084..16868751 (3333 bp), according Genome Release r6.36.

To generate the deletions, the plasmid construct was injected into embryos: y^1 *M{Act5C-Cas9.P.RFP-}ZH-2A* w^{1118} *DNAlig4[169]* (BL 58492 stock, Bloomington Drosophila Stock Center) together with two gRNAs. The F0 progeny were crossed with *y w*; *TM6/MKRS* flies. Flies with potential deletions were selected on the basis of dsRed-signal in the posterior part of their abdomens and these flies were crossed with *y w*; *TM6/MKRS* flies. All independently obtained flies with *dsRed* reporter were tested by PCR. The successful deletions events were confirmed by sequencing of PCR products. Next, *dsRed* reporter was deleted by Cre/*lox* recombination.

To create *M-*$i5^{attP}$ (SI Appendix, Fig. S4) the $i5^{1attP}$ and M^{3attP} were crossed with line expressing Cre recombinase (#1092, Bloomington Drosophila Stock Center). Then, $i5^{1attP}$/+; *CyO, P{w[+mC]=Crew}DH1/+* was crossed with M^{3attP}/+; *CyO, P{w[+mC]=Crew}DH1/+*. Next, the $i5^{1attP}/M^{3attP}$; *CyO, P{w[+mC]=Crew}DH1/+* males and females were crossed with each other and male offspring with the expected phenotypes were crossed with *y w*; *TM6/MKRS* flies. The deletion was confirmed by PCR and sequencing.

Generation of transgenic lines carrying different insertions in the *attP*-platforms.

The replacement vector was a plasmid with the *mini-yellow* and *mCherry* reporters as shown in SI Appendix, Fig. S1. The *iab-5* fragments were obtained by PCR amplification. Their coordinates are:

$i5^{1}$: 112812-113529; $i5^{2}$: 111101-113245; $i5^{3}$: 109349-111346; $i5^{4}$: 107265-109694; $i5^{5}$: 105709-107851; $i5^{5}$: 105030-105750; $i5^{7}$: 101629-104152; $i5^{ini}$: 104011-105035; $i5^{S1}$: 113227-113824; $i5^{S2}$: 112455-113245; $i5^{S3}$: 111607 - 112829; $i5^{S4}$: 104016 - 104537; $i5^{S5}$: 103516 - 104152; $i5^{S6}$: 101629 - 102685, according to the published sequences of the Bithorax complex (Martin et al., 1995).

Integration of the plasmids in the landing platforms was achieved by injecting the plasmid and a vector expressing the *ϕC31* recombinase into embryos of *yw;* $i5^{1attP}/i5^{1attP}$, or *yw;* M^{3attP}/M^{3attP}, or *yw; M-*

i5^{attP}*/M-i5*^{attP} lines. The successful integrations were selected on the basis of expression of *mini-y* in abdominal segments. The integration of the replacement DNA fragments was confirmed by PCR.

The *yellow* and *mCherry* reporters were excised by Cre-mediated recombination between the *lox* sites.

All stocks are available upon request.

Cuticle preparations

Cuticle preparations were carried out as described in (Postika et al., 2018).

Acknowledgements We are grateful to François Karch for discussing the results and editing the discussion. We thank Farhod Hasanov for fly injections, Kate O'Connor-Giles for *pHD-DsRed* plasmid (Addgene plasmid # 51434), Bloomington Drosophila Stock Center for Drosophila lines. We thank Natalia Klimenko for bioinformatics analysis.

Author contributions

P.G., O.K. designed experiments. O.K., N.P. performed experiments. P.S., P.G., O.K. wrote the main manuscript text. O.K. prepared figures. All authors reviewed the manuscript.

Competing interests

The authors declare no competing interests.

Funding

This work (all functional and morphological analysis) was supported by the Russian Science Foundation, project no. 19-14-00103 (to O.K.). Part of the genome editing procedure was supported by grant 075-15-2019-1661 from the Ministry of Science and Higher Education of the Russian Federation. P.S. would like to acknowledge support from NIH R35 GM126975.

References

Barges, S., Mihaly, J., Galloni, M., Hagstrom, K., Müller, M., Shanower, G., Schedl, P., Gyurkovics, H. and Karch, F. (2000). The Fab-8 boundary defines the distal limit of the bithorax complex iab-7 domain and insulates iab-7 from initiation elements and a PRE in the adjacent iab-8 domain. *Development* **127**, 779–790.

Bender, W. and Lucas, M. (2013). The border between the ultrabithorax and abdominal-A regulatory domains in the Drosophila bithorax complex. *Genetics* **193**, 1135–1147.

Bischof, J., Maeda, R. K., Hediger, M., Karch, F. and Basler, K. (2007). An optimized transgenesis system for Drosophila using germ-line-specific phiC31 integrases. *Proc Natl Acad Sci U S A* **104**, 3312–3317.

Bowman, S. K., Deaton, A. M., Domingues, H., Wang, P. I., Sadreyev, R. I., Kingston, R. E. and Bender, W. (2014). H3K27 modifications define segmental regulatory domains in the Drosophila bithorax complex. *Elife* **3**, e02833.

Busturia, A. and Bienz, M. (1993). Silencers in abdominal-B, a homeotic Drosophila gene. *The EMBO Journal* **12**, 1415–1425.

Camino, E. M., Butts, J. C., Ordway, A., Vellky, J. E., Rebeiz, M. and Williams, T. M. (2015). The evolutionary origination and diversification of a dimorphic gene regulatory network through parallel innovations in cis and trans. *PLoS Genet* **11**, e1005136.

Casares, F. and Sánchez-Herrero, E. (1995). Regulation of the infraabdominal regions of the bithorax complex of Drosophila by gap genes. *Development* **121**, 1855–1866.

Celniker, S. E., Sharma, S., Keelan, D. J. and Lewis, E. B. (1990). The molecular genetics of the bithorax complex of Drosophila: cis-regulation in the Abdominal-B domain. *EMBO J* **9**, 4277–4286.

Ciabrelli, F., Comoglio, F., Fellous, S., Bonev, B., Ninova, M., Szabo, Q., Xuéreb, A., Klopp, C., Aravin, A., Paro, R., et al. (2017). Stable Polycomb-dependent transgenerational inheritance of chromatin states in Drosophila. *Nat Genet* **49**, 876–886.

Couderc, J.-L., Godt, D., Zollman, S., Chen, J., Li, M., Tiong, S., Cramton, S. E., Sahut-Barnola, I. and Laski, F. A. (2002). The bric à brac locus consists of two paralogous genes encoding BTB/POZ domain proteins and acts as a homeotic and morphogenetic regulator of imaginal development in Drosophila. *Development* **129**, 2419–2433.

Crosby, M. A., Lundquist, E. A., Tautvydas, R. M. and Johnson, J. J. (1993). The 3' regulatory region of the Abdominal-B gene: genetic analysis supports a model of reiterated and interchangeable regulatory elements. *Genetics* **134**, 809–824.

Delorenzi, M. and Bienz, M. (1990). Expression of Abdominal-B homeoproteins in Drosophila embryos. *Development* **108**, 323–329.

Drewell, R. A., Nevarez, M. J., Kurata, J. S., Winkler, L. N., Li, L. and Dresch, J. M. (2014). Deciphering the combinatorial architecture of a Drosophila homeotic gene enhancer. *Mech Dev* **131**, 68–77.

Duncan, I. (1987). The bithorax complex. *Annu Rev Genet* **21**, 285–319.

Galloni, M., Gyurkovics, H., Schedl, P. and Karch, F. (1993). The bluetail transposon: evidence for independent cis-regulatory domains and domain boundaries in the bithorax complex. *EMBO J* **12**, 1087–1097.

Gao, G., McMahon, C., Chen, J. and Rong, Y. S. (2008). A powerful method combining homologous recombination and site-specific recombination for targeted mutagenesis in Drosophila. *Proc Natl Acad Sci U S A* **105**, 13999–14004.

Gyurkovics, H., Gausz, J., Kummer, J. and Karch, F. (1990). A new homeotic mutation in the Drosophila bithorax complex removes a boundary separating two domains of regulation. *EMBO J* **9**, 2579–2585.

Hagstrom, K., Muller, M. and Schedl, P. (1996). Fab-7 functions as a chromatin domain boundary to ensure proper segment specification by the Drosophila bithorax complex. *Genes Dev* **10**, 3202–3215.

Ho, M. C. W., Schiller, B. J., Goetz, S. E. and Drewell, R. A. (2009). Non-genic transcription at the Drosophila bithorax complex functional activity of the dark matter of the genome. *Int J Dev Biol* **53**, 459–468.

Hogga, I., Mihaly, J., Barges, S. and Karch, F. (2001). Replacement of Fab-7 by the gypsy or scs insulator disrupts long-distance regulatory interactions in the Abd-B gene of the bithorax complex. *Mol Cell* **8**, 1145–1151.

Iampietro, C., Gummalla, M., Mutero, A., Karch, F. and Maeda, R. K. (2010). Initiator elements function to determine the activity state of BX-C enhancers. *PLoS Genet* **6**, e1001260.

Jeong, S., Rokas, A. and Carroll, S. B. (2006). Regulation of body pigmentation by the Abdominal-B Hox protein and its gain and loss in Drosophila evolution. *Cell* **125**, 1387–1399.

Karch, F., Weiffenbach, B., Peifer, M., Bender, W., Duncan, I., Celniker, S., Crosby, M. and Lewis, E. B. (1985). The abdominal region of the bithorax complex. *Cell* **43**, 81–96.

Karch, F., Bender, W. and Weiffenbach, B. (1990). abdA expression in Drosophila embryos. *Genes Dev* **4**, 1573–1587.

Karch, F., Galloni, M., Sipos, L., Gausz, J., Gyurkovics, H. and Schedl, P. (1994). Mcp and Fab-7: molecular analysis of putative boundaries of cis-regulatory domains in the bithorax complex of Drosophila melanogaster. *Nucleic Acids Res* **22**, 3138–3146.

Kassis, J. A., Kennison, J. A. and Tamkun, J. W. (2017). Polycomb and Trithorax Group Genes in Drosophila. *Genetics* **206**, 1699–1725.

Kopp, A. and Duncan, I. (1997). Control of cell fate and polarity in the adult abdominal segments of Drosophila by optomotor-blind. *Development* **124**, 3715–3726.

Kopp, A., Duncan, I., Godt, D. and Carroll, S. B. (2000). Genetic control and evolution of sexually dimorphic characters in Drosophila. *Nature* **408**, 553–559.

Kuroda, M. I., Kang, H., De, S. and Kassis, J. A. (2020). Dynamic Competition of Polycomb and Trithorax in Transcriptional Programming. *Annu Rev Biochem* **89**, 235–253.

Kyrchanova, O., Toshchakov, S., Parshikov, A. and Georgiev, P. (2007). Study of the functional interaction between Mcp insulators from the Drosophila bithorax complex: effects of insulator pairing on enhancer-promoter communication. *Mol Cell Biol* **27**, 3035–3043.

Kyrchanova, O., Mogila, V., Wolle, D., Magbanua, J. P., White, R., Georgiev, P. and Schedl, P. (2015). The boundary paradox in the Bithorax complex. *Mech Dev* **138 Pt 2**, 122–132.

Kyrchanova, O., Mogila, V., Wolle, D., Deshpande, G., Parshikov, A., Cléard, F., Karch, F., Schedl, P. and Georgiev, P. (2016). Functional Dissection of the Blocking and Bypass Activities of the Fab-8 Boundary in the Drosophila Bithorax Complex. *PLoS Genet* **12**, e1006188.

Kyrchanova, O., Zolotarev, N., Mogila, V., Maksimenko, O., Schedl, P. and Georgiev, P. (2017). Architectural protein Pita cooperates with dCTCF in organization of functional boundaries in Bithorax complex. *Development* **144**, 2663–2672.

Kyrchanova, O., Sabirov, M., Mogila, V., Kurbidaeva, A., Postika, N., Maksimenko, O., Schedl, P. and Georgiev, P. (2019a). Complete reconstitution of bypass and blocking functions in a minimal artificial Fab-7 insulator from Drosophila bithorax complex. *Proc Natl Acad Sci U S A* **116**, 13462–13467.

Kyrchanova, O., Wolle, D., Sabirov, M., Kurbidaeva, A., Aoki, T., Maksimenko, O., Kyrchanova, M., Georgiev, P. and Schedl, P. (2019b). Distinct Elements Confer the Blocking and Bypass Functions of the Bithorax Fab-8 Boundary. *Genetics* **213**, 865–876.

Kyrchanova, O., Maksimenko, O., Ibragimov, A., Sokolov, V., Postika, N., Lukyanova, M., Schedl, P. and Georgiev, P. (2020). The insulator functions of the Drosophila polydactyl C2H2 zinc finger protein CTCF: Necessity versus sufficiency. *Sci Adv* **6**, eaaz3152.

Lewis, E. B. (1978). A gene complex controlling segmentation in Drosophila. *Nature* **276**, 565–570.

Maeda, R. K. and Karch, F. (2015). The open for business model of the bithorax complex in Drosophila. *Chromosoma* **124**, 293–307.

Martin, C. H., Mayeda, C. A., Davis, C. A., Ericsson, C. L., Knafels, J. D., Mathog, D. R., Celniker, S. E., Lewis, E. B. and Palazzolo, M. J. (1995). Complete sequence of the bithorax complex of Drosophila. *Proc Natl Acad Sci U S A* **92**, 8398–8402.

Massey, J. H. and Wittkopp, P. J. (2016). The Genetic Basis of Pigmentation Differences Within and Between Drosophila Species. *Curr Top Dev Biol* **119**, 27–61.

McCall, K., O'Connor, M. B. and Bender, W. (1994). Enhancer traps in the Drosophila bithorax complex mark parasegmental domains. *Genetics* **138**, 387–399.

Mihaly, J., Hogga, I., Barges, S., Galloni, M., Mishra, R. K., Hagstrom, K., Muller, M., Schedl, P., Sipos, L., Gausz, J., et al. (1998). Chromatin domain boundaries in the Bithorax complex. *Cellular and Molecular Life Sciences (CMLS)* **54**, 60–70.

Mihaly, J., Barges, S., Sipos, L., Maeda, R., Cléard, F., Hogga, I., Bender, W., Gyurkovics, H. and Karch, F. (2006). Dissecting the regulatory landscape of the Abd-B gene of the bithorax complex. *Development* **133**, 2983–2993.

Müller, J. and Bienz, M. (1992). Sharp anterior boundary of homeotic gene expression conferred by the fushi tarazu protein. *EMBO J* **11**, 3653–3661.

Peifer, M., Karch, F. and Bender, W. (1987). The bithorax complex: control of segmental identity. *Genes Dev* **1**, 891–898.

Postika, N., Metzler, M., Affolter, M., Müller, M., Schedl, P., Georgiev, P. and Kyrchanova, O. (2018). Boundaries mediate long-distance interactions between enhancers and promoters in the Drosophila Bithorax complex. *PLoS Genet* **14**, e1007702.

Postika, N., Schedl, P., Georgiev, P. and Kyrchanova, O. (2021). Mapping of functional elements of the Fab-6 boundary involved in the regulation of the Abd-B hox gene in Drosophila melanogaster. *Sci Rep* **11**, 4156.

Qian, S., Capovilla, M. and Pirrotta, V. (1991). The bx region enhancer, a distant cis-control element of the Drosophila Ubx gene and its regulation by hunchback and other segmentation genes. *EMBO J* **10**, 1415–1425.

Rebeiz, M. and Williams, T. M. (2017). Using Drosophila pigmentation traits to study the mechanisms of cis-regulatory evolution. *Curr Opin Insect Sci* **19**, 1–7.

Roeske, M. J., Camino, E. M., Grover, S., Rebeiz, M. and Williams, T. M. (2018). Cis-regulatory evolution integrated the Bric-à-brac transcription factors into a novel fruit fly gene regulatory network. *Elife* **7**,.

Sánchez-Herrero, E. (1991). Control of the expression of the bithorax complex genes abdominal-A and abdominal-B by cis-regulatory regions in Drosophila embryos. *Development* **111**, 437–449.

Shimell, M. J., Simon, J., Bender, W. and O'Connor, M. B. (1994). Enhancer point mutation results in a homeotic transformation in Drosophila. *Science* **264**, 968–971.

Shimell, M. J., Peterson, A. J., Burr, J., Simon, J. A. and O'Connor, M. B. (2000). Functional analysis of repressor binding sites in the iab-2 regulatory region of the abdominal-A homeotic gene. *Dev Biol* **218**, 38–52.

Simon, J., Peifer, M., Bender, W. and O'Connor, M. (1990). Regulatory elements of the bithorax complex that control expression along the anterior-posterior axis. *EMBO J* **9**, 3945–3956.

Simon, J., Chiang, A. and Bender, W. (1992). Ten different Polycomb group genes are required for spatial control of the abdA and AbdB homeotic products. *Development* **114**, 493–505.

Starr, M. O., Ho, M. C. W., Gunther, E. J. M., Tu, Y.-K., Shur, A. S., Goetz, S. E., Borok, M. J., Kang, V. and Drewell, R. A. (2011). Molecular dissection of cis-regulatory modules at the Drosophila bithorax complex reveals critical transcription factor signature motifs. *Dev Biol* **359**, 290–302.

Wang, W., Kidd, B. J., Carroll, S. B. and Yoder, J. H. (2011). Sexually dimorphic regulation of the Wingless morphogen controls sex-specific segment number in Drosophila. *Proc Natl Acad Sci U S A* **108**, 11139–11144.

Williams, T. M., Selegue, J. E., Werner, T., Gompel, N., Kopp, A. and Carroll, S. B. (2008). The regulation and evolution of a genetic switch controlling sexually dimorphic traits in Drosophila. *Cell* **134**, 610–623.

Zhou, J., Barolo, S., Szymanski, P. and Levine, M. (1996). The Fab-7 element of the bithorax complex attenuates enhancer-promoter interactions in the Drosophila embryo. *Genes Dev* **10**, 3195–3201.

Figures

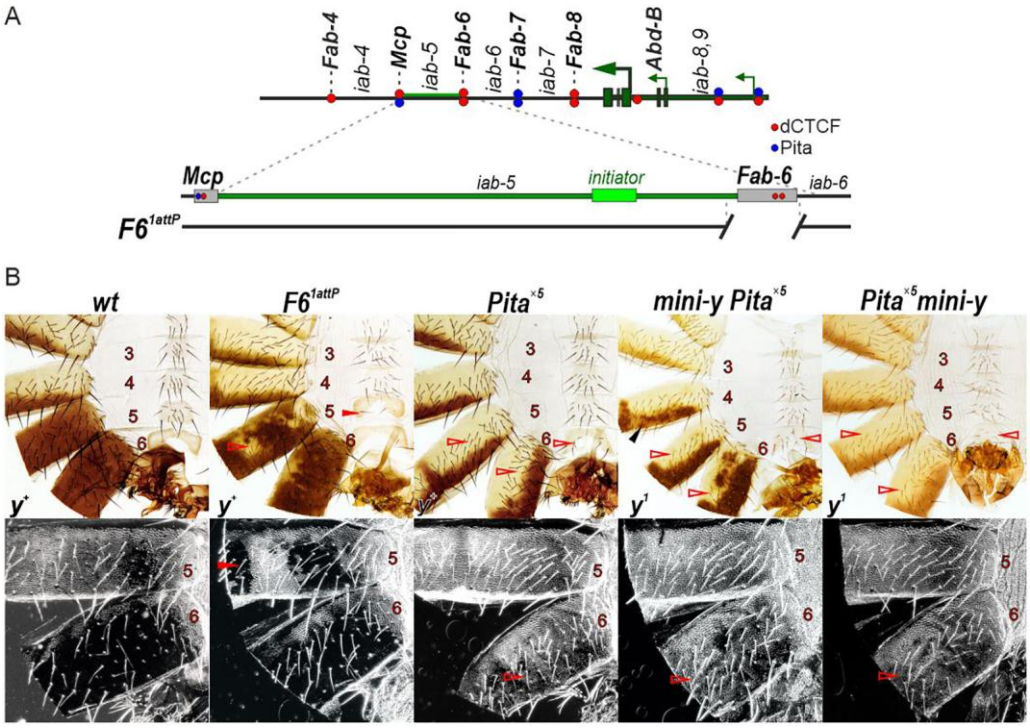

Figure 1. The substitution of the *Fab-6* boundary by Pita sites blocks the *Abd-B* expression in the A5 and A6 segments. (A) Scheme of the *Abd-B* regulatory region and the $F6^{1attP}$ deletion. The *Abd-B* promoters are shown by green arrows. The dashed lines with colored circles mark boundaries. Pita and dCTCF are indicated by blue and red circles, respectively. The DNAse I hypersensitive sites of *Mcp* and *Fab-6* boundaries are shown as grey boxes. The endpoints of the $F6^{1attP}$ deletion used in the replacement experiments are indicated by breaks in the black lines. (B) Morphology of the male abdominal segments (numbered) in *wt*, $F6^{1attP}$ and $Pita^{\times 5}$ lines. In $Pita^{\times 5}$ replacements males the A6 sternite has an intermediate form between quadrilateral (as in *wt* A5) and banana-like (as in *wt* A6) and is partially covered by bristles, while the tergite loses pigmentation and is covered by trichomes. The filled red arrowheads show morphological features indicative of GOF transformations. The empty red arrowheads show LOF transformations. Black arrowheads indicate pigmented spots that are induced by the *mini-y* expression. The localization of trichomes on the A5 and A6 tergites are shown in dark field.

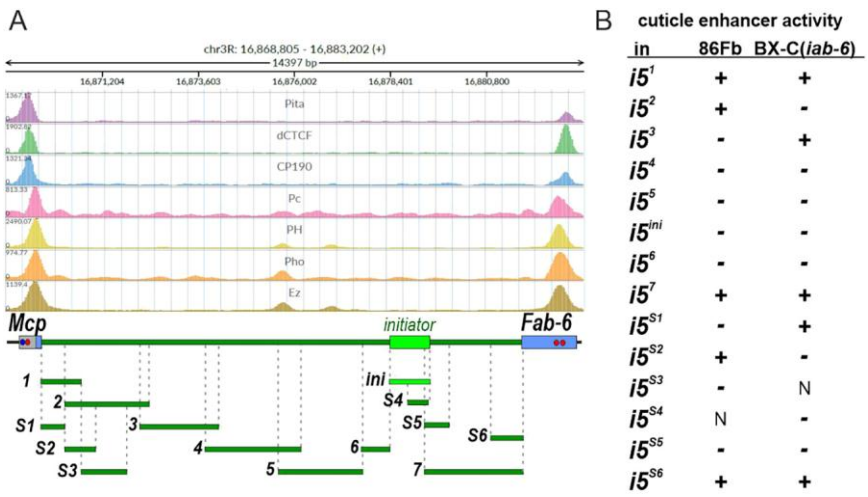

Figure 2. Summarize results of testing the *iab-5* DNA fragments for enhancer activity in 86Fb region and the *iab-6* region. (A) Molecular maps of the *iab-5* DNA fragments tested for enhancer activity. The binding of architectural (Pita, dCTCF and CP190) and Polycomb (Pc, PH, Pho, Ez) proteins are shown above the scheme of the *iab-5* domain. The PREs (Polycomb Response Elements) were mapped from distal side of the *Mcp* boundary and in the *Fab-6* boundary. The Polycomb proteins are also weakly bound to the region overlapped with $i5^4$ and $i5^5$. The raw data were taken from the datasets presented in Table S1. Signal of protein binding RPKM normalized and averaged using 50bps bin size. (B) Summarize results of mapping enhancers in the *iab-5* regulatory domain in 86Fb region and in the *iab-6* domain of BX-C. "+", the tested fragment is able to activate transcription; "-", the fragment is not able to activate transcription, N, no data.

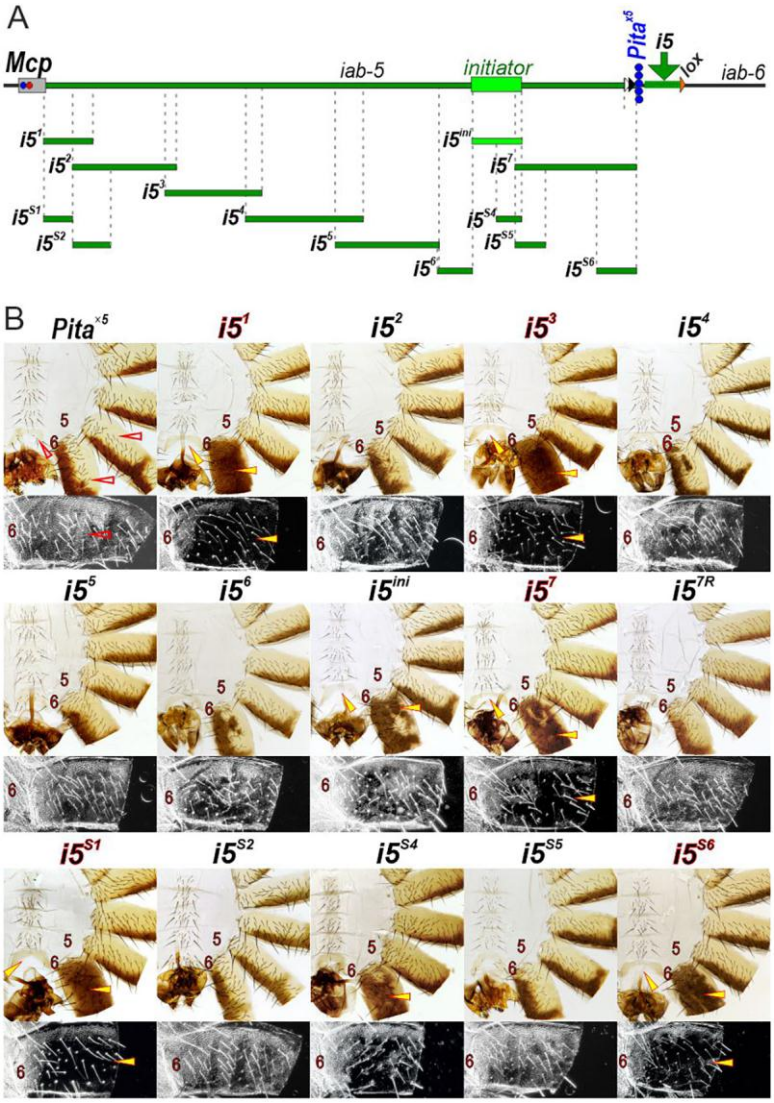

Figure 3. Testing regions in the *iab-5* domain that stimulate *Abd-B* expression in the A6 segment. (A) Scheme of *iab-5* with the Pita$^{\times5}$ replacements in the *F6*^{1attP} platform. The *i5* fragments tested for enhancer activity are shown as green lines, the *i5*^{ini} fragment including the initiator is shown as light green line. The test fragments were integrated near *Pita*$^{\times5}$ (five blue circles vertically) in the *iab-6* domain. (B) Morphology of male abdominal segments in transgenic lines with different *Pita*$^{\times5}$*-i5* substitutions. The localization of trichomes in the A6 tergite is shown in dark field. The yellow arrowheads show the signs of rescue the LOF phenotype in A6. All other designations are the same as in Fig. 1.

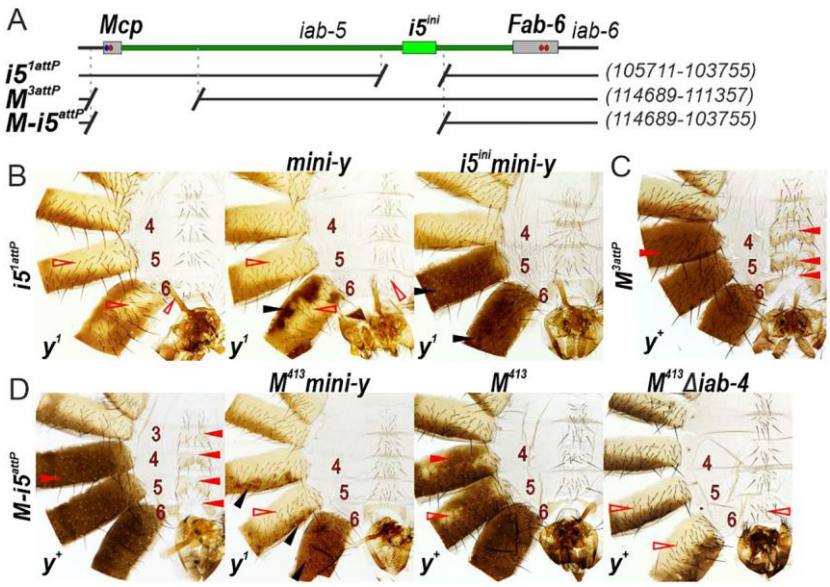

Figure 4. Deletions in the *iab-5* and *iab-4* domains. (A) Scheme of the $i5^{1attP}$, M^{3attP} and $M\text{-}i5^{attP}$ deletions. The endpoints of the deletions are indicated by breaks in the black lines. The coordinates of endpoints are according to the complete sequence of BX-C in SEQ89E numbering (Martin et al., 1995). Morphology of the male abdominal segments in transgenic line carrying (B) the $i5^{1attP}$ deletion with (y^1; $i5^{1attP}$*mini-y*) or without (y^1; $i5^{1attP}$) the *mini-y* reporter or with re-integration of the 1019 bp *iab-5* initiator and the *mini-y* reporter ($i5^{ini}$*mini-y*); (C) the M^{3attP} platform; (D) the $M\text{-}i5^{attP}$ platform, integration of the M^{413} insulator in $M\text{-}i5^{attP}$ with (M^{413}*mini-y*) or without (M^{413}) *mini-y*, deletion of the *iab-4* region in M^{413} ($M^{413}\Delta$*iab-4*). Designations are the same as in Fig. 1.

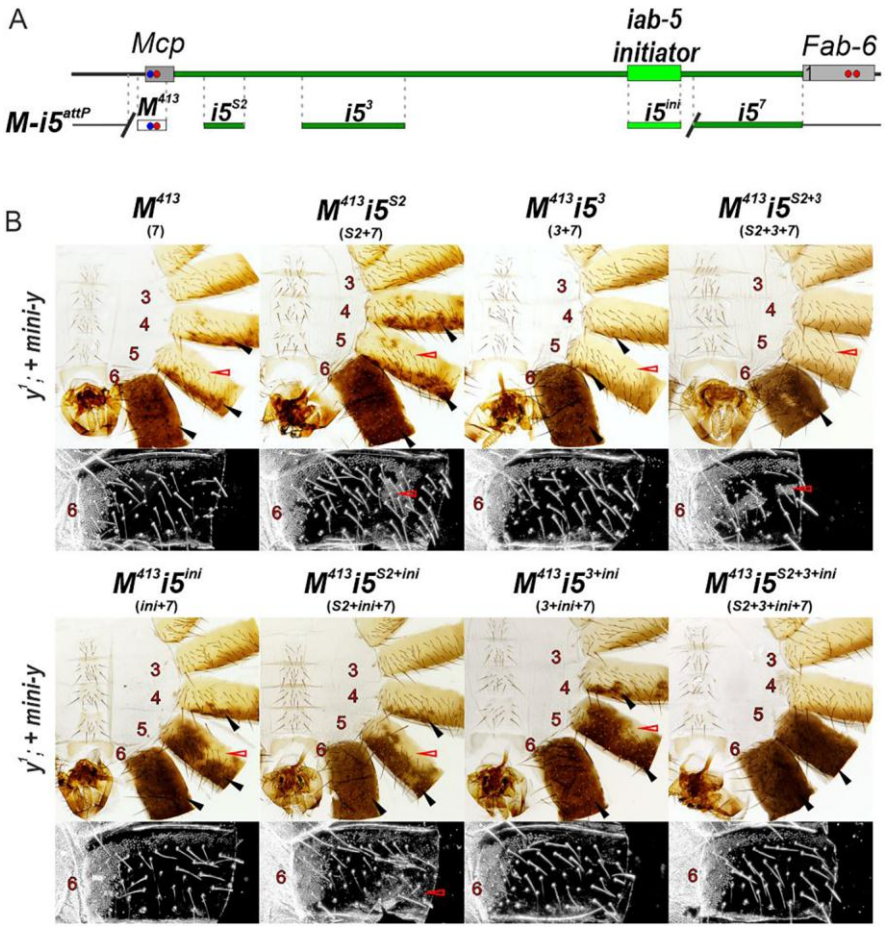

Figure 5. Reconstruction of the *iab-5* domain with *i5* fragments integrated in the *M-i5*^{attP} platform. (A) Scheme of the *M-i5*^{attP} platform and derivative lines carrying insertion of different *i5* combinations with the *M*^{413}. (B) Morphology of the male abdominal segments in transgenic line carrying the *M-i5*^{attP} and different combination of *i5* fragments with the *M*^{413}. In all transgenic lines the *mini-y* and *mCherry* reporters are present. Designations are the same as described in Fig. 1.

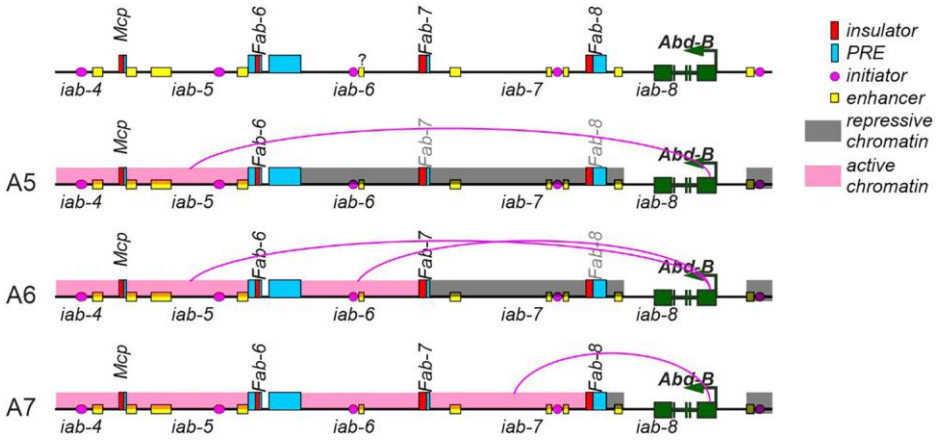

Figure 6. Schematic presentation of *Abd-B* activation by *iab-5*, *iab-6* and *iab-7* in A5, A6 and A7 segments correspondingly. Magenta arcs indicates interactions domain enhancers with *Abd-B* promoter.

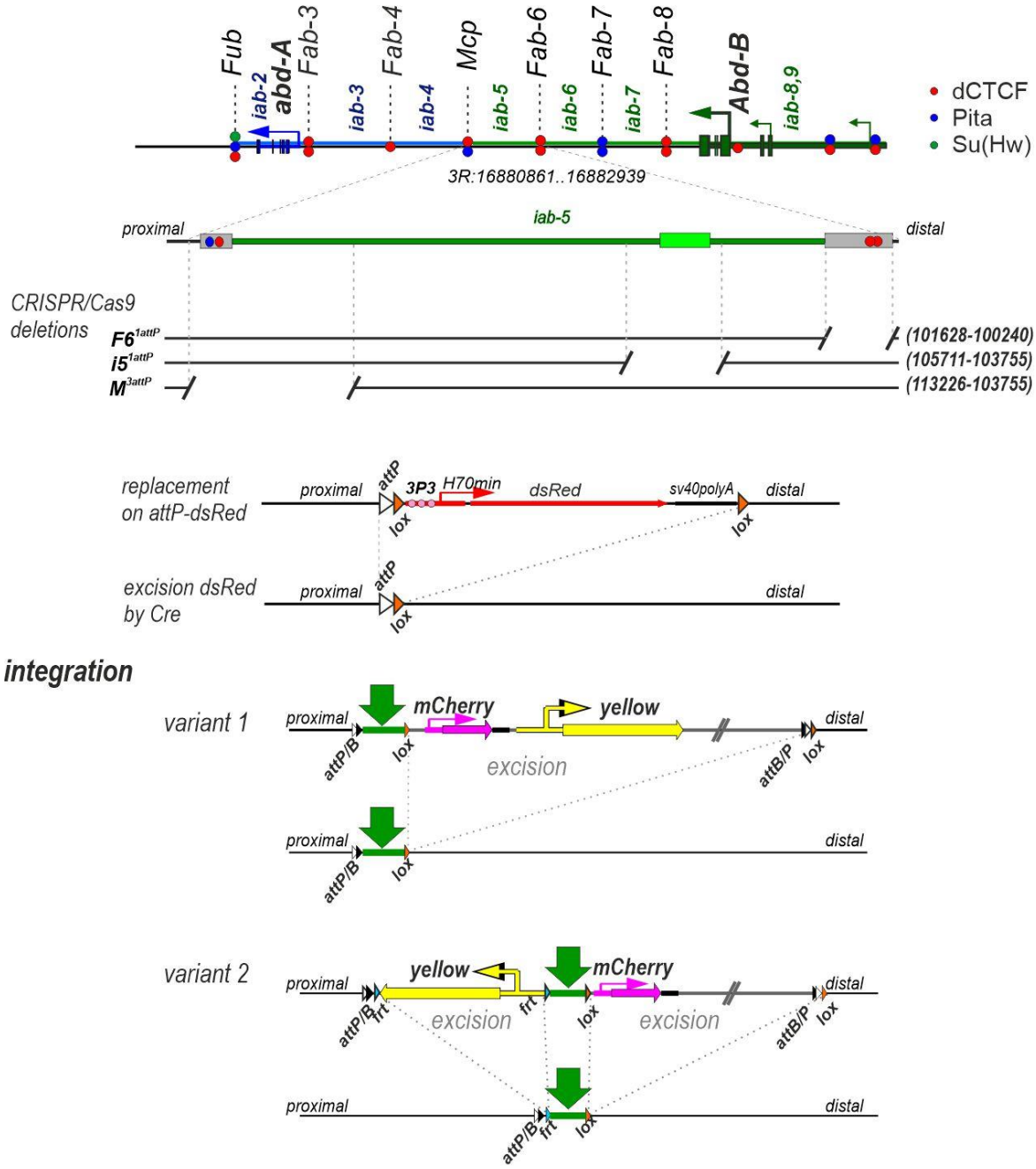

Fig. S1. **Strategy for generating deletions using CRISPR/Cas9 technology.** Scheme of the *abd-A* and *Abd-B* regulatory regions and *iab-5* domain. The *abd-A* and *Abd-B* promoters are indicated as blue and green arrows, correspondingly. The DNAse I hypersensitive sites of *Mcp* and *Fab-6* boundaries are indicated as gray boxes. The dashed lines with colored circles mark boundaries. Pita and dCTCF are indicated by blue and red circles, respectively. The coordinates of the endpoints of the $F6^{1attP}$, $i5^{1attP}$, M^{3attP} deletions (shown as breaks in the black lines) are according to the complete sequence of BX-C in SEQ89E numbering (Martin et al. 1995). The deletions were obtained by substituting the designated DNA sequences with an *attP* site (white triangle) and flanked by *lox* sites (orange triangle) the *dsRed* reporter (thick red arrow) with *3P3* promoter and SV40 terminator (thick black line). To remove *dsRed* the recombination between the *lox* sites was used. The replacement vector plasmids have the *mini-yellow* (thick yellow arrow) and *mCherry* (thick magenta arrow) reporters. Downward thick green arrow indicates testing element insertion.

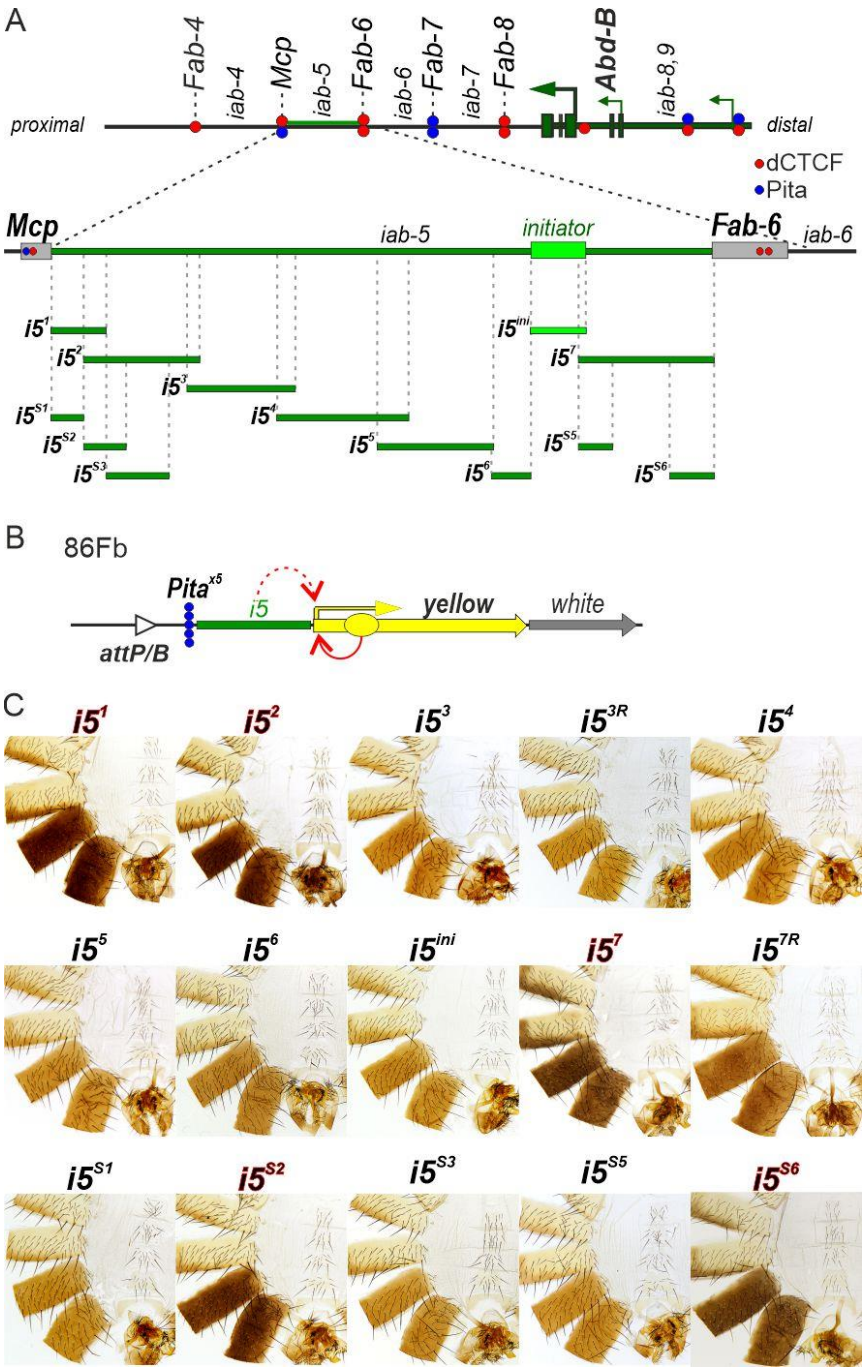

Fig. S2. Mapping the enhancers in the *iab-5* domain that are able to stimulate the *mini-y* reporter in the 86Fb landing site. (A) The scheme of the *Abd-B* regulatory region and the *iab-5* domain. The tested *i5* fragments are shown as green lines, $i5^{ini}$ that includes the initiator is shown as light green line. (B) The model construct for testing enhancer activity with *yellow* (marked by yellow arrow) and *mini-white* (grey arrow) genes has *attB* site for integration. The *yellow* required for cuticle pigmentation was used without wing and body enhancers. Enhancer of bristles located in intron was used as marker of *yellow* promotor activity. The *white* reporter was used to identify transformation events. To reduce potential position effects, we placed $Pita^{\times 5}$ (five blue circles) upstream of the *i5* fragments. (C) Photos of male abdominal segments in the y^1 background.

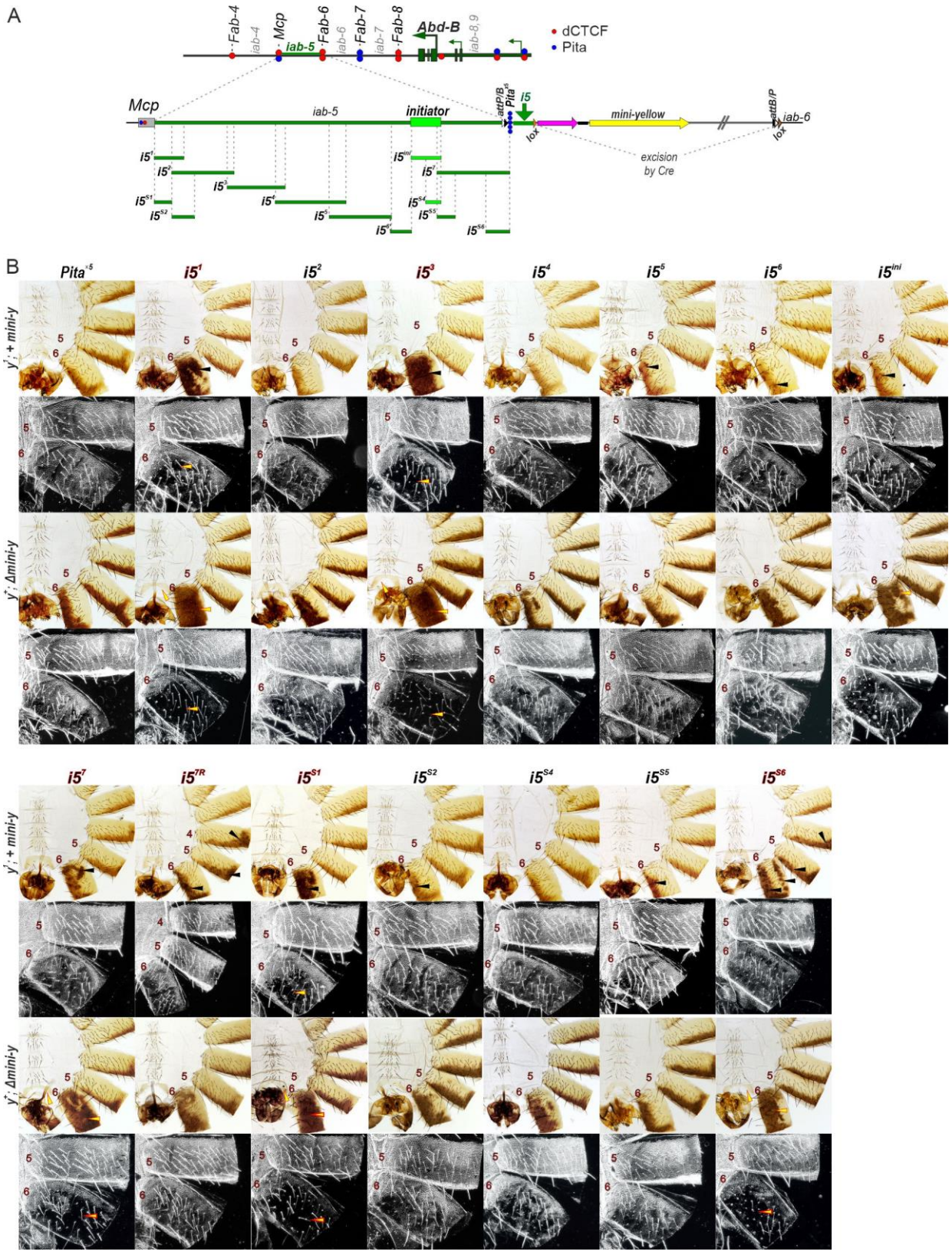

Fig. S3. Testing *iab-5* fragments for *Abd-B* activation in the cuticle of the A6 segment. (A) Scheme of the *Abd-B* regulatory region and *iab-5* domain with the $Pita^{\times 5}$ replacement construct integrated in the $F6^{1attP}$ platform. The *i5* fragments testing for the enhancer activity (green lines), or the $i5^{ini}$ including the initiator (light green line) are integrated near $Pita^{\times 5}$ (five blue circles) in the *iab-6* domain. The *mCherry* under control of minimal *hs70* promoter (magenta arrow) and the *mini-y* (yellow arrow) are flanked by *lox* sites (orange arrows). The Cre-mediated recombination between *lox* sites results in the deletion of both reporters. (B) Morphology of the male abdominal segments of the obtained lines in presence (y^1; *mini-y*) or absence (y^+; *Δmini-y*) of the reporters. Black arrowheads indicate pigmented spots that are induced by the *mini-y* expression. The yellow arrowheads show the signs of rescue the LOF phenotype in A6. The localization of trichomes on the 5th to 6th abdominal tergites are shown in dark field.

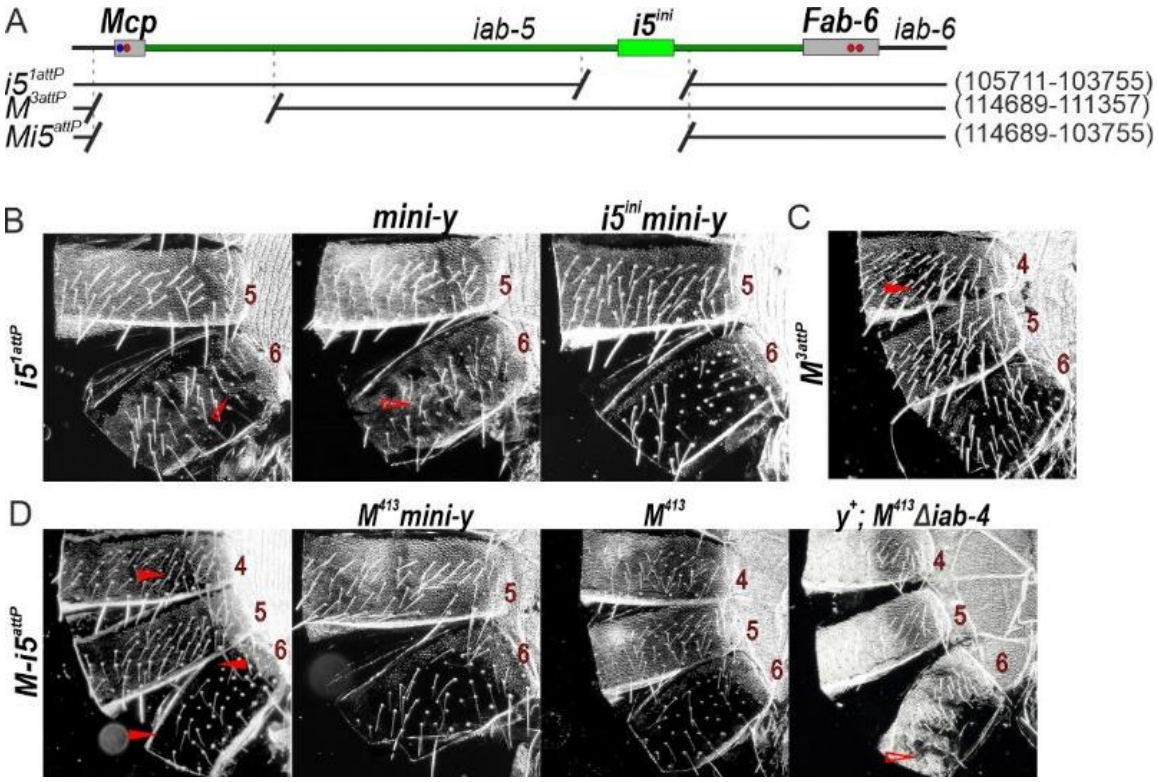

Fig. S4. Deletions in the *iab-5* and *iab-4* domains. (A) Scheme of the $i5^{1attP}$, M^{3attP} and $Mi5^{attP}$ deletions. The endpoints of the deletions are indicated by breaks in the black lines. The coordinates of endpoints are according to the complete sequence of BX-C in SEQ89E numbering (Martin et al. 1995). (B-D) Morphology in dark field of the male abdominal segments in obtained platforms and substitutions. (B) The $i5^{1attP}$ platform with reintegration of *mini-y* reporter or with combination of $i5^{ini}$+*mini-y*. (C) The M^{3attP} platform. (D) The *M-*$i5^{attP}$ platform and its derivatives (see in the text). Designations are the same as described in Fig.S3.

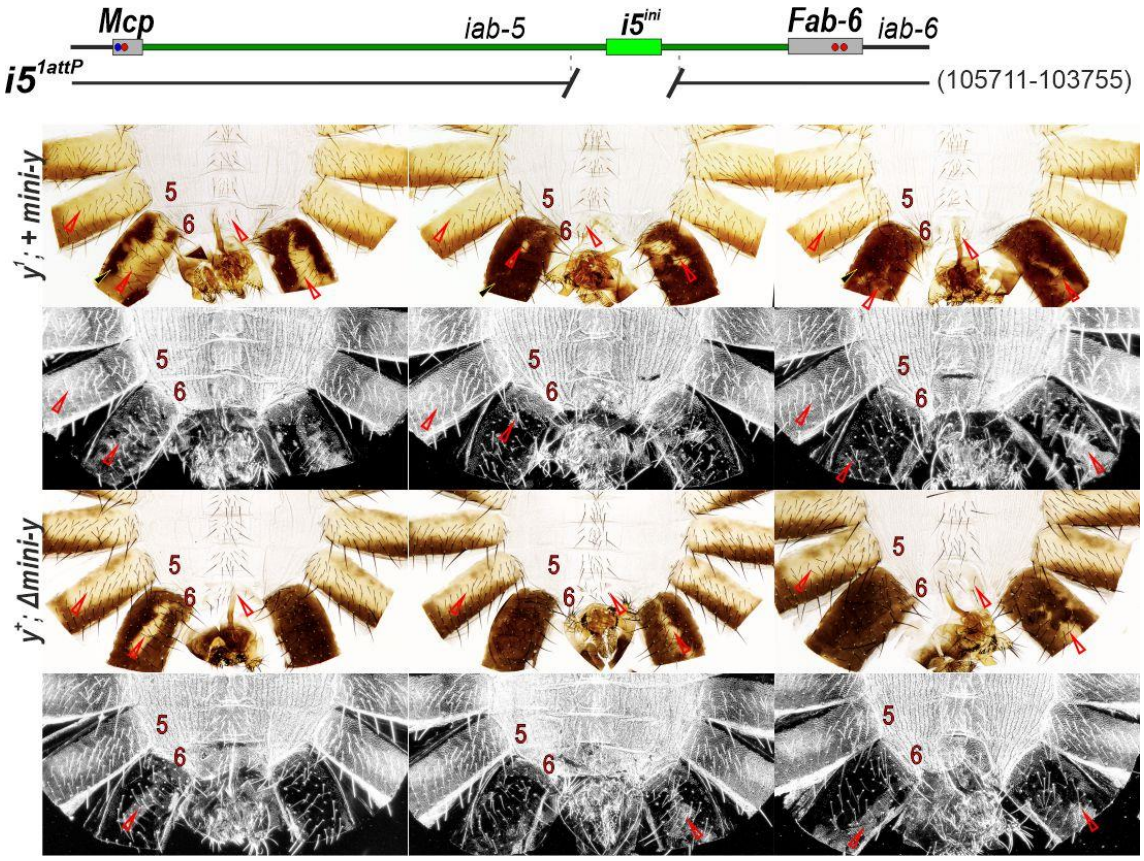

Fig. S5. Variation of *i5*^{attP} phenotype in males.

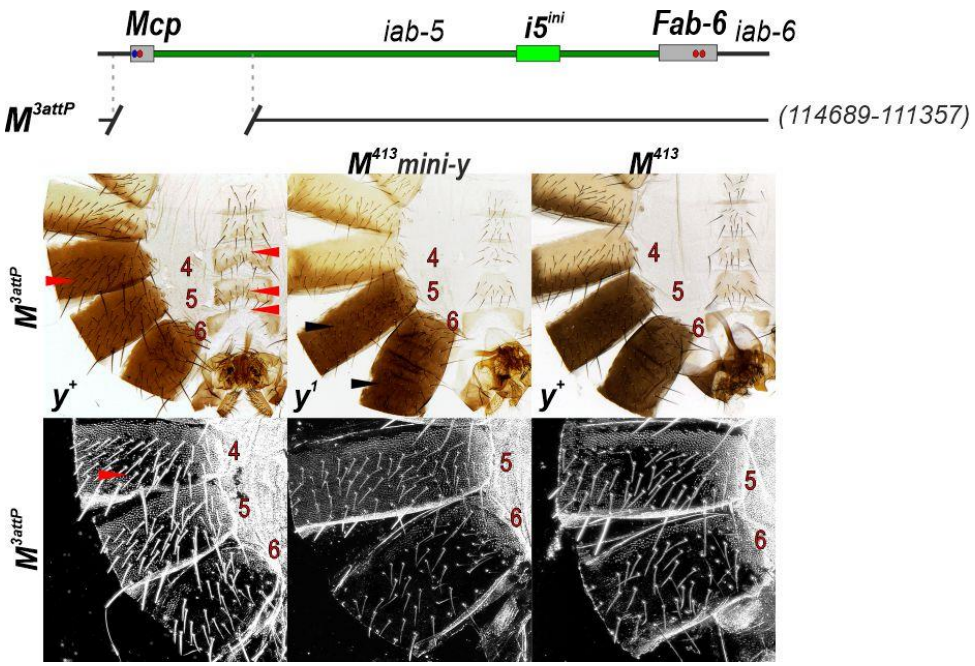

Fig. S6. *Mcp*^{413} can rescue 3333 bp deletion of *Mcp*. *Mcp*^{413} effectively isolate *mini-y* reporter in A5 segment. After deletion reporters *Mcp*^{413} almost completely restore *wt* phenotype. Designations are the same as described in Fig.S3.

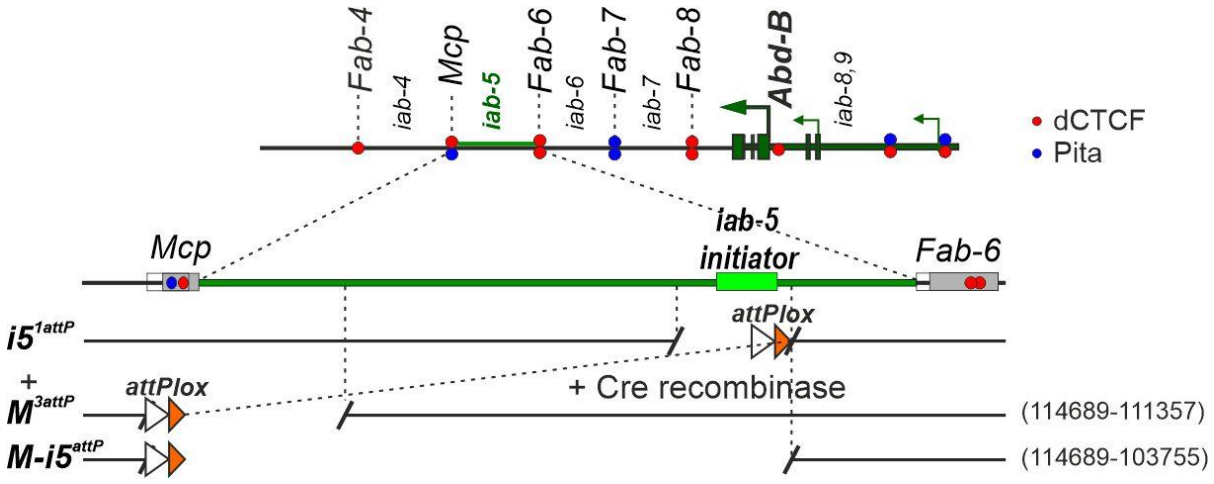

Fig. S7. Scheme for generating of the *M-i5*^{attP} deletion. The *i5*^{1attP}/*M*^{3attP} trans heterozygote was combined with the line expresses Cre recombinase (#1092, Bloomington Drosophila Stock Center). Cre-mediated recombination resulted in a deletion named *M-i5*^{attP} (dominant GOF phenotype in the male A4 segment). Other designations are as in the Fig. S1.

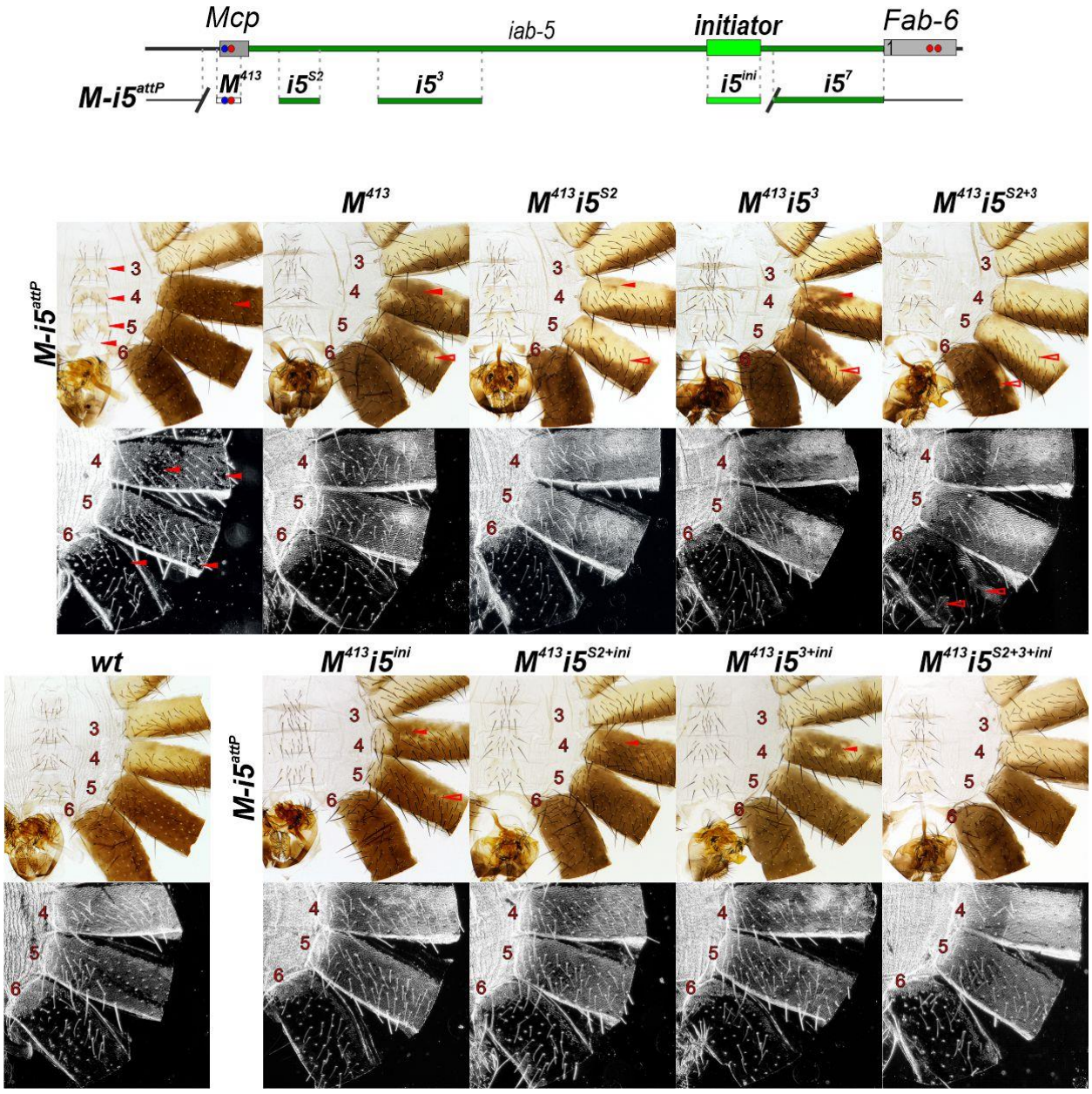

Fig. S8. Reconstruction of the *iab-5* domain with *i5* fragments. (A) Scheme of the *M-i5*^{attP} platform and *i5* fragments used in combination with the 413 bp *Mcp* insulator (*M*^{413}) for reconstitution of the *iab-5* domain. (B) Morphology of male abdominal segments in lines integrated into *M-i5*^{attP} without of the *mini-y* and *mCherry* reporters. Designations are the same as described in Fig.S3.

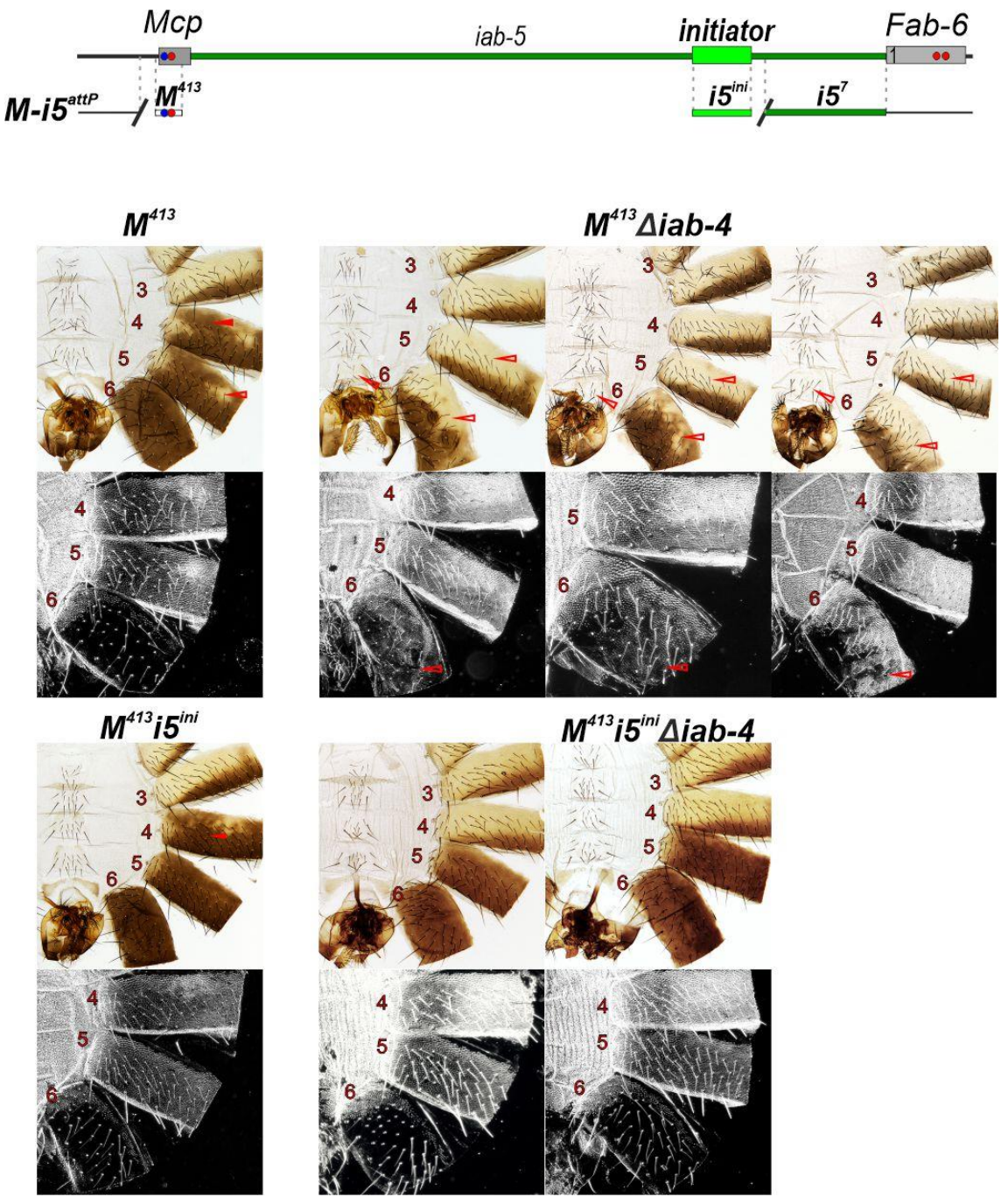

Fig. S9. Variation of the A6 phenotype in male after *iab-4* deletion in M^{413} and M^{413}+$i5^{ini}$ without of the *mini-y* and *mCherry* reporters (M-$i5^{attP}$ platform).

Table S1. List of datasets of proteins

	tissue	antibody	GEO/ENCODE link
PHO	E6-18h	PHO	https://www.ncbi.nlm.nih.gov/geo/query/acc.cgi?acc=GSM1479972
PH	E6-18h	PH	https://www.ncbi.nlm.nih.gov/geo/query/acc.cgi?acc=GSM2211686
Pc	E6-18h	PC	https://www.ncbi.nlm.nih.gov/geo/query/acc.cgi?acc=GSM1479973
E(z)	third instar larval imaginal discs and brains	E(z)	https://www.ncbi.nlm.nih.gov/geo/query/acc.cgi?acc=GSM2734944
Kr	E16-24h	KW3-Kr-D2	https://www.ncbi.nlm.nih.gov/geo/query/acc.cgi?acc=GSM636835
Hb	Blastoderm	HB	https://www.ncbi.nlm.nih.gov/geo/query/acc.cgi?acc=GSM1228851
Ftz	E0-24h	ftz-f1-GFP	https://www.encodeproject.org/biosamples/ENCBS313WAD/
Kni	E8-16h	KW3-kni-D2	https://www.ncbi.nlm.nih.gov/geo/query/acc.cgi?acc=GSM570045
Eve	E1-6h	eGFP-eve	https://www.encodeproject.org/experiments/ENCSR550SQH/
CP190	E5-13h	CP190	https://www.ncbi.nlm.nih.gov/geo/query/acc.cgi?acc=GSM1481701

CTCF and Pita as in Maksimenko et al.,2015